A6.2 Assessment and pilot strategy on the use of remote sensing to supplement traditional monitoring methods

19.12.2025

LIFE20 IPE/FI/000020 LIFE-IP BIODIVERSEA

Co-funded by the European Union. Views and opinions expressed are however those of the author(s) only and do not necessarily reflect those of the European Union or CINEA. Neither the European Union nor the granting authority can be held responsible for them.

Assessment and pilot strategy on the use of remote sensing to supplement traditional monitoring methods

Ari-Pekka Jokinen[1], Eero Alkio[1], Sakari Väkevä[1], Joni Koskikala[2], Pekka Lehtonen[2], Ari Laine[2], Charlotta Björklund[3], Louise Forsblom[1]

[1]Finnish Environment Institute
[2]Parks and Wildlife Finland
[3]Government of Åland

Contents

Aims

The aim of this task is to identify and develop remote sensing methods that can be used to supplement conventional monitoring techniques in the monitoring of marine habitats in the Finnish sea area. This deliverable specifically highlights the advantages and limitations of these methods. The marine habitats selected for remote sensing piloting mainly consist of submerged habitat forming species and are thus of great interest when assessing the marine state, conservation and restoration efforts. In addition to the submerged habitats, we also consider coastal reed beds as they can both form mosaics rich in underwater biodiversity, as well as expand, driven by eutrophication, and outcompete more sensitive species.

Even with challenges including, water turbidity, and weather conditions, remote sensing methods have the potential of capturing changes over large spatial scale in a cost-efficient manner, but capturing the full extent requires joint use with acoustic methods (Forsblom et al. 2024).

Introduction

Suitable imagery for mapping aquatic vegetation can be acquired from several sources with varying spatial and spectral resolutions. Publicly available satellite imagery such as Sentinel-2 and Landsat programs offer imagery with medium to high spatial resolution of 15-10 meters and spectral range from the visual wavelengths to far infrared. Commercial optical satellite imagery comes with varying sensors yet offers higher spatial resolution (typically in range 0.3-5 meters) than Sentinel-2 or Landsat and usually covers at least the visible wavelengths and near infrared. Aerial orthophotos are regularly collected every few years for the same area by National Land Survey of Finland (NLS) which are publicly available and offer sub-meter spatial resolution but are distributed as 8-bit RGB images. However, the aerial images offer an open data source to observe detailed information about the aquatic vegetation cover and fragmentation. Finally, drones can acquire imagery at ultrahigh detail with centimetre-scale spatial resolution, but the extent of the mapped area is most limited. Drones carry most often a common RGB camera, but multi- and hyperspectral sensors are also available.

Observing submerged aquatic vegetation (SAV) via optical remote sensing sensors is limited by absorption of electromagnetic radiation in the water column. Hence, water quality, colour and water transparency affect how light is absorbed, transmitted and reflected in the water and what can be observed. In general, wavelengths beyond visible light are quickly absorbed by water. Considering this, optical remote sensing methods for mapping underwater aquatic vegetation are not equally applicable to all areas in Finnish coastal waters. Also, detecting the lower growth limit of vegetation is often difficult to determine from optical remote sensing imagery due to limited water transparency. Acoustic sonar sensors can be used to complement optical imagery or to map areas where water quality prevents the use of airborne remote sensing and therefore acoustic methods have been piloted as well. However, similarly to drone data, the areal extent that is feasible to map is limited.

Material and methods for targeted habitats

Finnish marine biodiversity has been mapped for the past 20 years in the VELMU inventory programme (Forsblom et al. 2024) which provides substantial amount of in-situ point observations. This data is used as a baseline to target remote sensing monitoring to certain habitats (Table 1). As the inventory data may have large temporal offset to remote sensing imagery, additional field work has also been conducted in piloting remote sensing methods to reduce the temporal mismatch between in-situ and remote sensing observations.

Table 1. Habitats and piloted remote sensing methods

Habitat	Objective	Method	Scale
Reed beds	Extent monitoring	Satellite remote sensing, Bayesian data analysis	National
Seagrass meadow	Extent, condition	Drones, Aerial photos, Satellite remote sensing, Acoustic methods	Local or regional
Fucus beds	Extent, condition	Drones, Satellite remote sensing, acoustic methods	Local or regional
Sheltered stonewort habitats (lagoon)	Extent	Drones	Local
Exposed stonewort habitats	Extent	Aerial photos, Satellite remote sensing, acoustic methods	Local or regional

Coastal reeds (*Phragmites* sp., *Typha* spp., *Schoenoplectus* spp.)

This activity focused on the detection of emergent macrophytes of the red-list habitat R04 Coastal reeds. The detection is based on soil-adjusted vegetation index (SAVI) and distance from shore. SAVI measures the reflectivity of vegetation at near-infrared to the reflectivity at red wavelengths but does not saturate at high values as quickly as the more typical normalized-difference vegetation index (NDVI). Leafy vegetation stands out from water in terms of SAVI (and NDVI) because water strongly absorbs infrared radiation, whereas leaves reflect it to protect the plant from overheating. The method used for this activity was originally developed during Blue Carbon Habitats project (2021) financed by Nordic Council of Ministers – Ocean and Climate Group (Koponen et al. 2022) and improved during BlueLakes project (RRF-funding, 2024–2025) for inland waters and now Biodiversea A6 for coastal habitats. Whereas these previous applications of the method used NDVI, the evolutions carried out under Biodiversea are the first to use SAVI.

The coastal reeds detection method is not limited to strictly monospecific stands of common reed (*Phragmites australis*) but can be sensitive to other emergent macrophytes growing in shallow water near the coastline (e.g., bulrushes, sedges). However, the detection method has been trained with *Phragmites* data, and since the common reed has large horizontally growing leaves, they typically have characteristically high SAVI (and NDVI) values since they obscure the visibility to the water surface when viewed from above. Therefore, it is expected and also known from previous experiments, that most of the areas mapped by this method still represent stands of common reed.

Input data. We downloaded reflectance band mosaics for Sentinel-2 satellite for the full mission (2016–2025) from the S2GM service (https://s2gm.land.copernicus.eu/), yearly time periods between 15 June to 15 August in a 10-m spatial resolution. Next, we computed the yearly SAVI index maps from these data for all areas that lie strictly within the sea areas as defined by the Velmu sea mask. We also computed a 'proximity raster' in the same spatial scale and with the same spatial extent as the SAVI rasters, where each pixel tells the Euclidean distance to the nearest shoreline in meters. These two variables, SAVI and distance, were used as the input features for the classification method.

For in situ data of reed occurrence, we used the monospecific *Phragmites* sp. observations from Velmu field inventory data. We clustered the observations to find the ~25 most extensive reed areas of the dataset and used very-high resolution satellite imagery (Copernicus Contributing Missions, VHR Image 2018, 2021, and 2024 datasets) and aerial orthophoto interpretation (National Land Survey) to digitize the outer margins of the reed belts. Next, we marked points along these margins at every 60 m segments and extracted 3×3 windows of NDVI data around the points. This resulted in ~20,000 sampling points of roughly 50:50 composition of reeds and non-reeds. The non-reeds could in this case include the open water areas adjacent to reed belts, sparse stands of helophytes, or macrophytes presenting another growth form (e.g., nymphaeids and elodeids).

We also randomly chose 100 monospecific *Phragmites* sp. stands from the Velmu inventory data and used the same imagery as described above to digitise the thicknesses of the reed belts in direction perpendicular to the coastline.

Method. Our methodological assumptions are that reed belts' thicknesses are distributed as $t \sim \mathrm{Exp}(\lambda)$, the SAVIs of non-reed and reed are distributed as $X_{\mathrm{non-reed}} \sim N(\mu_{\mathrm{non-reed}}, \sigma^2_{\mathrm{non-reed}})$ and $X_{\mathrm{reed}} \sim N(\mu_{\mathrm{reed}}, \sigma^2_{\mathrm{reed}})$, and that at a random location at the shoreline, the shore hosts vegetation at a constant probability C. With these assumptions, we use a Naïve Bayes (NB) -like method to predict the posterior log-likelihood $\ell_{\mathrm{reed}}(x, d|\theta)$ of a new observation (x, d) (where x is SAVI and d distance from shore) representing coastal reeds, against it representing non-reeds. The log-likelihood is interpreted in this way: the value $\ell_{\mathrm{reed}} = 0$ represents the decision threshold, $\ell_{\mathrm{reed}} > 0$ that reed is more likely than non-reed, and $\ell_{\mathrm{reed}} < 0$ that non-reed is more likely than reed. Here, θ represents the parameters on which the interpretation is conditioned, namely $\mu_{\mathrm{non-reed}}$, $\sigma^2_{\mathrm{non-reed}}$, μ_{reed}, σ^2_{reed}, λ, and C. Other parameters can be derived from the data empirically, but C has proved to be difficult to measure. Therefore, we optimized C to give a maximally 50:50 separation between reeds and non-reeds in the training dataset, whereas other parameters were fixed to their empirically determined values.

This part of the work is also being worked on in a scientific manuscript (Väkevä et al., in progress). Queries about the exact methodology can be directed to the lead author.

Results. Based on our empirical data, the reed belt thickness scaling length is $\lambda^{-1} = 35.7\ \mathrm{m}$. This means that the median thickness of reed belts is $\ln 2 \cdot \lambda^{-1} \approx 10.7\ \mathrm{m}$. Therefore, about half of the coastal reeds are less than 1 pixel wide in the Sentinel-2 data, making their detection uncertain. Fitting a bimodal normal distribution in the SAVI values of the training dataset gives $\mu_{\mathrm{non-reed}} = 0.01$, $\sigma_{\mathrm{non-reed}} = 0.16$, $\mu_{\mathrm{reed}} = 0.54$, and $\sigma_{\mathrm{reed}} = 0.15$, with the component weights $w_{\mathrm{non-reed}} = 0.50$ and $w_{\mathrm{reed}} = 0.50$. The empirical distributions of the data are seen in Figure 1. Using $\ell_{\mathrm{reed}} = 0$ as the decision threshold for classification and $\lambda^{-1} = 30.0\ \mathrm{m}$ as the scale parameter, we ended up using the value $C = 0.40$ because it gave a sufficient

separation between reed and non-reed targets in the training dataset, and increasing it further did not considerably change the log-likelihood values nor the final classification.

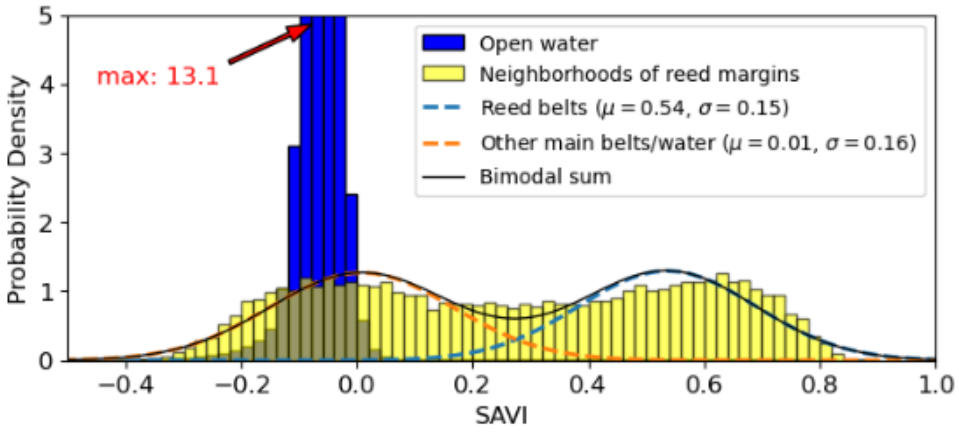

Figure 1: Distribution of SAVI index at the neighborhoods of reed margins (yellow histogram) and in open-water areas further away from the shoreline (blue histogram). The neighborhoods of reed margins are composed of reed and non-reed pixels in roughly 50:50 proportion. The fitted bi-modal normal distribution is shown as a black curve and its components in green and orange dashed curves. Our method essentially probes the likelihood of an observed SAVI value to belong to the right component (reeds) in the bi-modal distribution, against it belonging to the left component (other main belts/water), and also takes into account the pixel's distance from the closest seashore.

The log-likelihood interpretation of coastal reed occurrence is exemplified over a demonstration area in Southwestern Finland in Figure 2. It is seen that the method separates well and objectively reed targets from non-reed targets and is also sensitive to reed belts in various stages of succession. $\ell = 0$ turns out to be a fairly good discriminant between reeds and non-reeds.

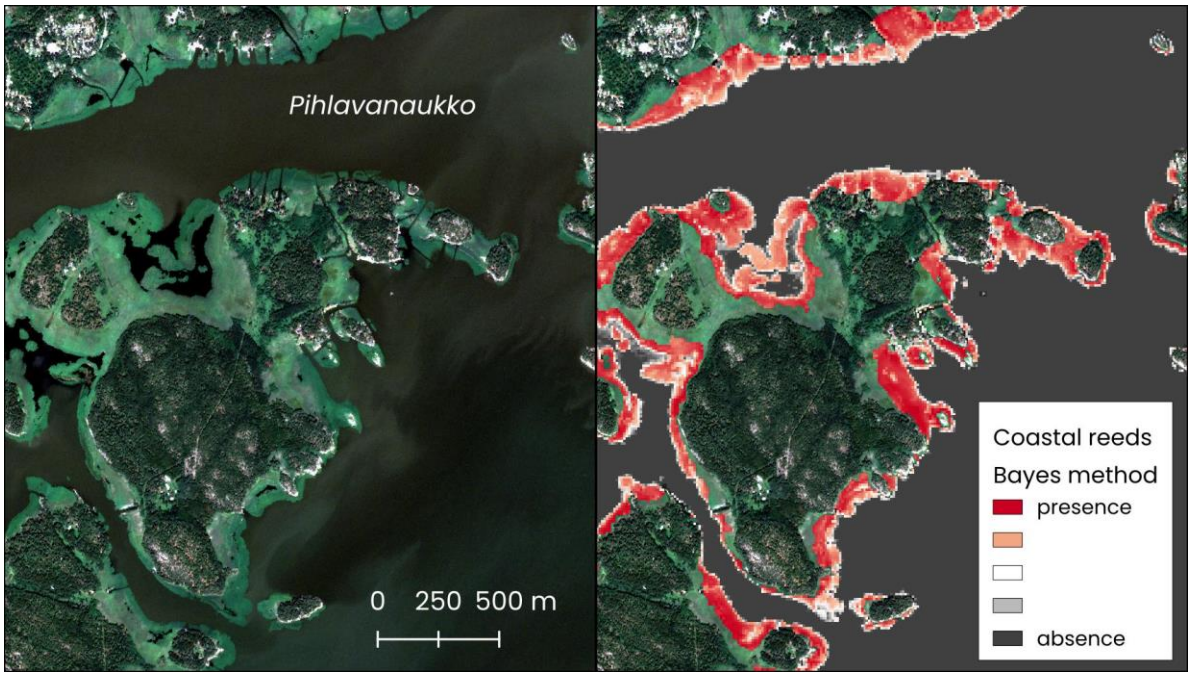

Figure 2: Left: true-colour Pléiades-1B image from the Baltic Sea coast in the municipality of Vehmaa, Southwestern Finland, in 2 July 2024. Contains modified Copernicus Contributing Mission data from the IMAGE2024 collection. Right: Same scene, overlaid with the log-likelihood of Sentinel-2 mapped pixels representing coastal reeds. The decision threshold ($\ell = 0$) is indicated in white colour, and reddening colours have increasing likelihoods of representing coastal reeds ($\ell > 0$). Contains modified Copernicus Sentinel-2 data, Syke (2025). Note that the method does not account for the landward side of the shoreline.

The bar chart in Figure 3 shows the annual time series of reed belt total areas over the duration of the Sentinel-2 mission. Here, reeds are defined as pixels with $\ell > 0$, and their total area is simply the count of pixels multiplied by $10\ \mathrm{m} \times 10\ \mathrm{m}$ (the area of a single pixel). As a comparison, the red bars show the reed total areas computed using the method that is implemented in the CORINE Land Cover classification. The Bayes method predicts larger total areas for the Finnish coast, on average.

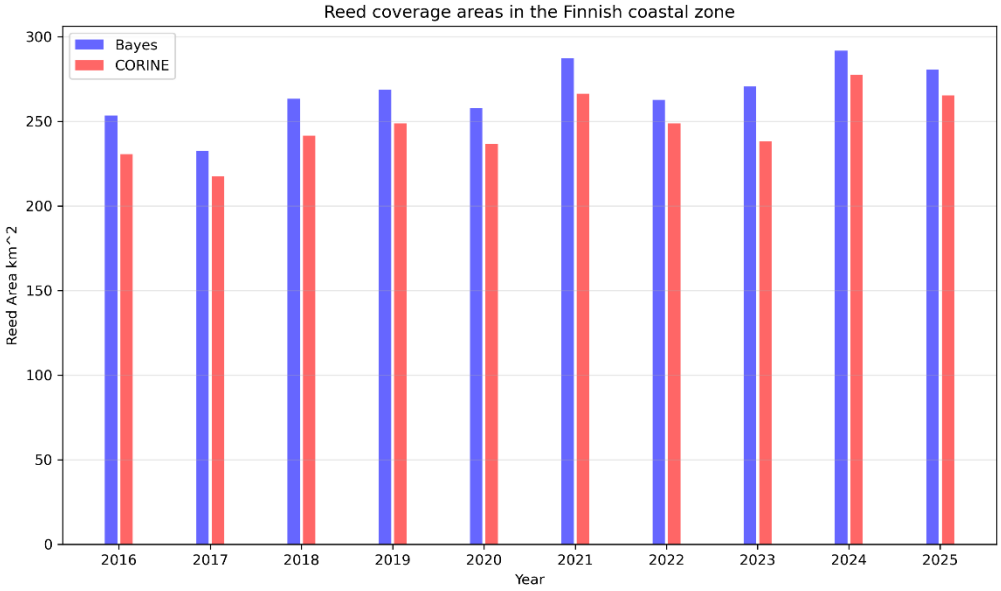

Figure 3: Annual time series of total reed belt area along the Finnish coast during the Sentinel-2 mission. Bayes = this work, CORINE = reference method used for producing the Salt marshes (aquatic) land use class of the Finnish CORINE Land Cover dataset in 2025 (M. Törmä et al., pers. comm.).

Summary. The Bayesian method enables the generation of an annual time series that aligns well with the CORINE reference approach. However, it is more objective as it relies on few adjustable parameters, most of which can be derived directly from remote-sensing data without auxiliary field sampling. Compared to CORINE, the method is simpler to apply as it requires only two reflectance channels and does not depend on water depth information. Since it is a probabilistic classification framework, it also opens possibilities for mapping other main belts of macrophytes; the user can shift the decision boundary to accept more uncertain areas as vegetation.

Like all methods based on vegetation index mosaics, the method is sensitive to data availability and cloudiness throughout the year, which can cause irregular boundaries in the posterior probability estimates even within homogeneous macrophyte stands. This is particularly well seen in 2016 and 2017 when Sentinel-2 mission only had one satellite in operation. It also requires a sea-shore mask and cannot detect reed beds on the landward side of the shoreline. The shoreline in national geodatabases typically represents mean-water conditions, but practical water-level fluctuations can expose or submerge vast areas of the shore. Reed beds extending far from the shoreline (>500 m) may be misclassified as unlikely reed areas because even very high SAVI values do not give enough support to convince the method that the pixel is not a cloud error.

While the method can provide preliminary identification of coastal reed stands in a broad sense, species-level accuracy remains limited and may require complementary approaches (e.g., reflectance time series analysis). Further development especially for the scientific publication should focus on comprehensive, data-driven validation and the regional trend analysis within the provinces of Finland.

Seagrass meadows

Southern coast of Hanko peninsula hosts some of the largest seagrass meadows on the Finnish coast and therefore the area is most suitable for piloting different monitoring methods. Besides the main seagrass species *Zostera marina*, the meadows consist other vascular plants and algae, forming mixed communities. These meadows are clearly visible from good quality remote sensing imagery where the SAV in general can be mapped. Detailed data collection in small areas within Kolaviken was made for estimating the amount of *Zostera marina* within the meadow. Other piloting efforts focused on mapping the SAV extent from optical remote sensing and how underwater acoustic methods may complement these in defining the lower growth limit and vegetation height.

SAV mapping from optical satellite remote sensing

Data and methods

Drop-video and dive point observations from Velmu inventory dataset were used together with additional field observations collected from Kolaviken (Figure 4). The vegetation coverage from the point observations was aggregated to form classification labels so that points with total vegetation cover < 30 were considered bare or low vegetation, >= 30 as SAV, and all points with depth > 6 meters as deep water. The point labelling was additionally evaluated visually against different resolution satellite images because of temporal offset between the points and satellite images, and to exclude points where observation contradicted what was visually interpretable from image.

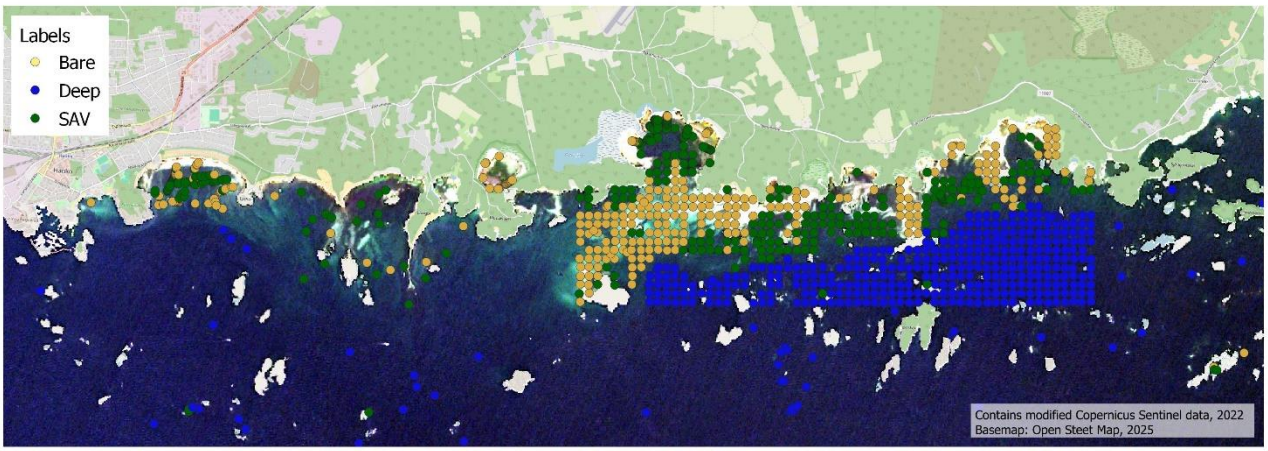

Figure 4. Map of the pilot area with labeled point observations

Image classification was made following object-based image analysis (OBIA) principle where an image segmentation algorithm is used to form clusters (or segments) of adjacent pixels that share similar values. The points are then overlaid over the segments and habitat defined for the whole segment based on the point observations. These segments of pixels and their corresponding masks of semantic classes were then used in training machine learning algorithms for classification. Three common algorithms, namely Random Forest (RF), Support Vector Machine (SVM) and Extreme Gradient Boosting (XGB) were compared. 10-fold stratified grouped K-fold cross-validation was used to split the data to train and test sets and evaluate the model. Models were evaluated using common metrics: overall accuracy, producer's accuracy (precision) and user's accuracy (recall). Grouping was done on segment level so that pixels within a segment could either be only in train or test set. This was done to account for spatial autocorrelation of pixel values and to better estimate the generalizability of the model. This workflow was tested both on very-high resolution WV-2 satellite image (taken 20.07.2022) as openly available Sentinel-2 satellite image (taken 21.07.2022).

Results

All the ML algorithms showed similar performance, average overall accuracy being between 90-95% for WV-2, and around 85% for Sentinel-2. Main differences between the models are visible in amount of variance in performance between different folds and semantic classes (Figure 5, Figure 6).

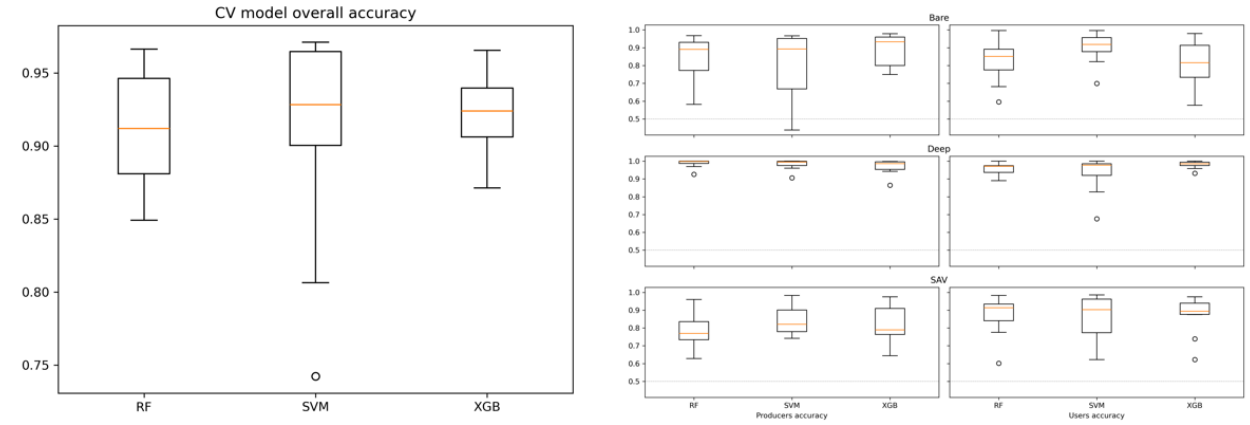

Figure 5. Model performance comparison from 10-fold stratified K-fold estimation for WV-2 image classification

Deep water class showed lowest variance between the folds whereas bare sediment and SAV classes had higher variance.

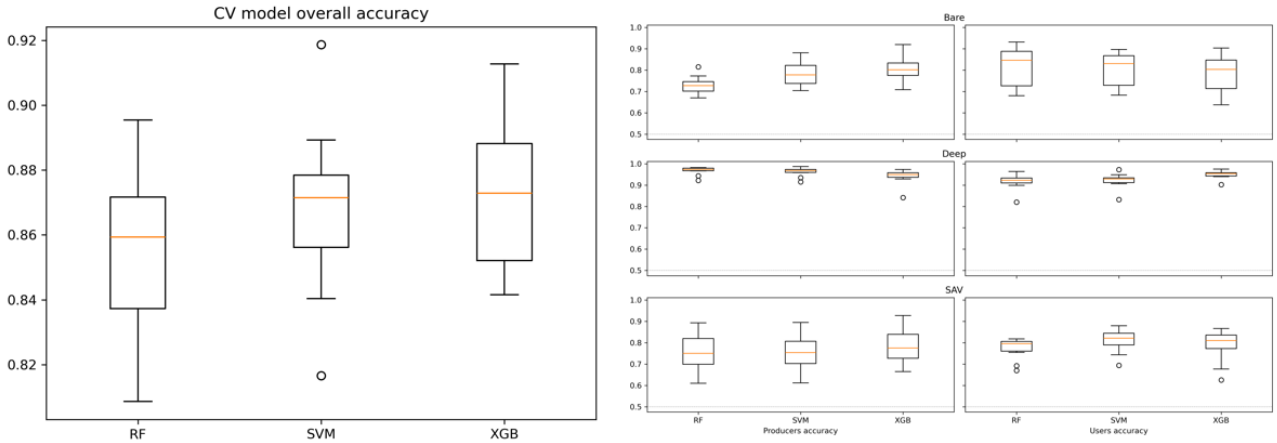

Figure 6. Model performance comparison from 10-fold stratified K-fold estimation for Sentinel-2 image classification

Prediction map examples (Figure 7, Figure 8) show XGB classification probabilities above 0,75 for SAV for the different resolution WV-2 and Sentinel-2 satellite images.

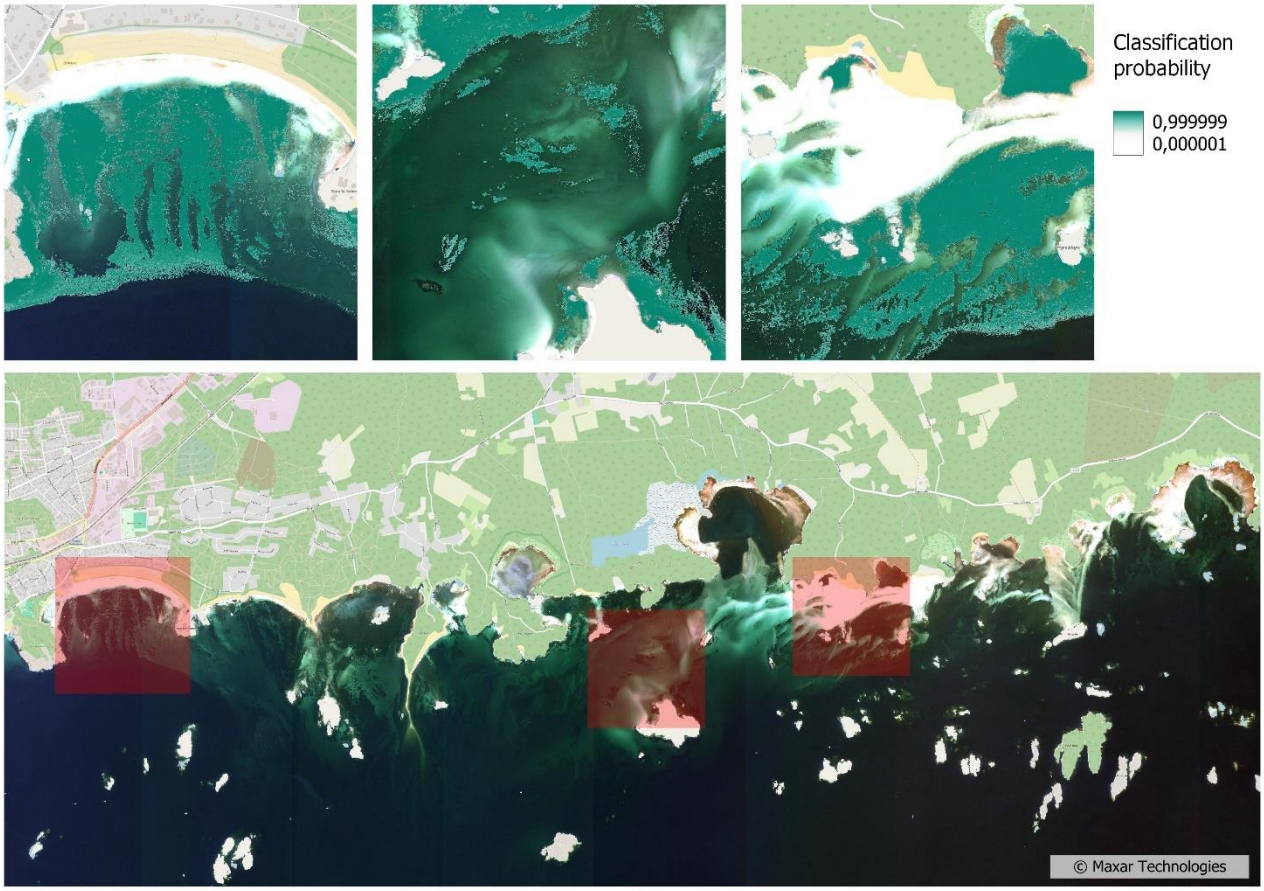

Figure 7. Mapping of SAV extent from WorldView-2 satellite image. Smaller images show examples of classification probability for SAV for each subarea from left to right respectively. Bottom image shows the RGB visualization of the Worldview-2 over the study area. Probabilities below 0,75 are cut off for visualization purposes

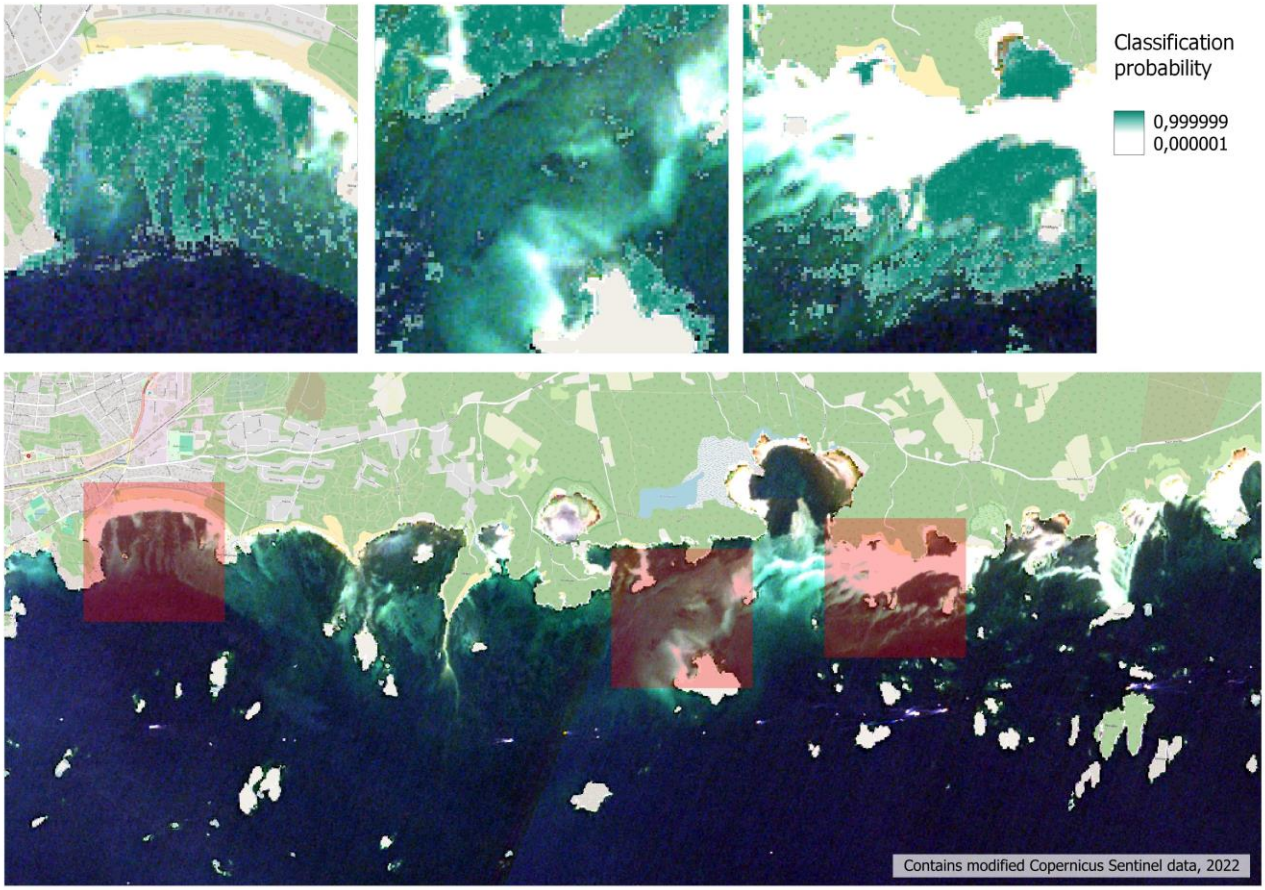

Figure 8. Mapping of SAV extent from Sentinel-2 satellite image. Smaller images show examples of classification probability for SAV for each subarea from left to right respectively. Bottom image shows the RGB visualization of the Sentinel-2 over the study area. Probabilities below 0,75 are cut off for visualization purposes.

Area comparison of the prediction results from the two different spatial resolution sensors shows higher area estimates for the VHR image (Figure 9). For smaller subareas the area estimates show larger differences whereas the area estimate for the larger region shows about 17% difference. Differences may be explained by 1) better classification accuracy near the edges of vegetation patches in VHR image and therefore larger area cover, 2) better classification accuracy and/or overestimation near the deep water threshold which seems more conservative in Sentinel-2 prediction based on visual estimate.

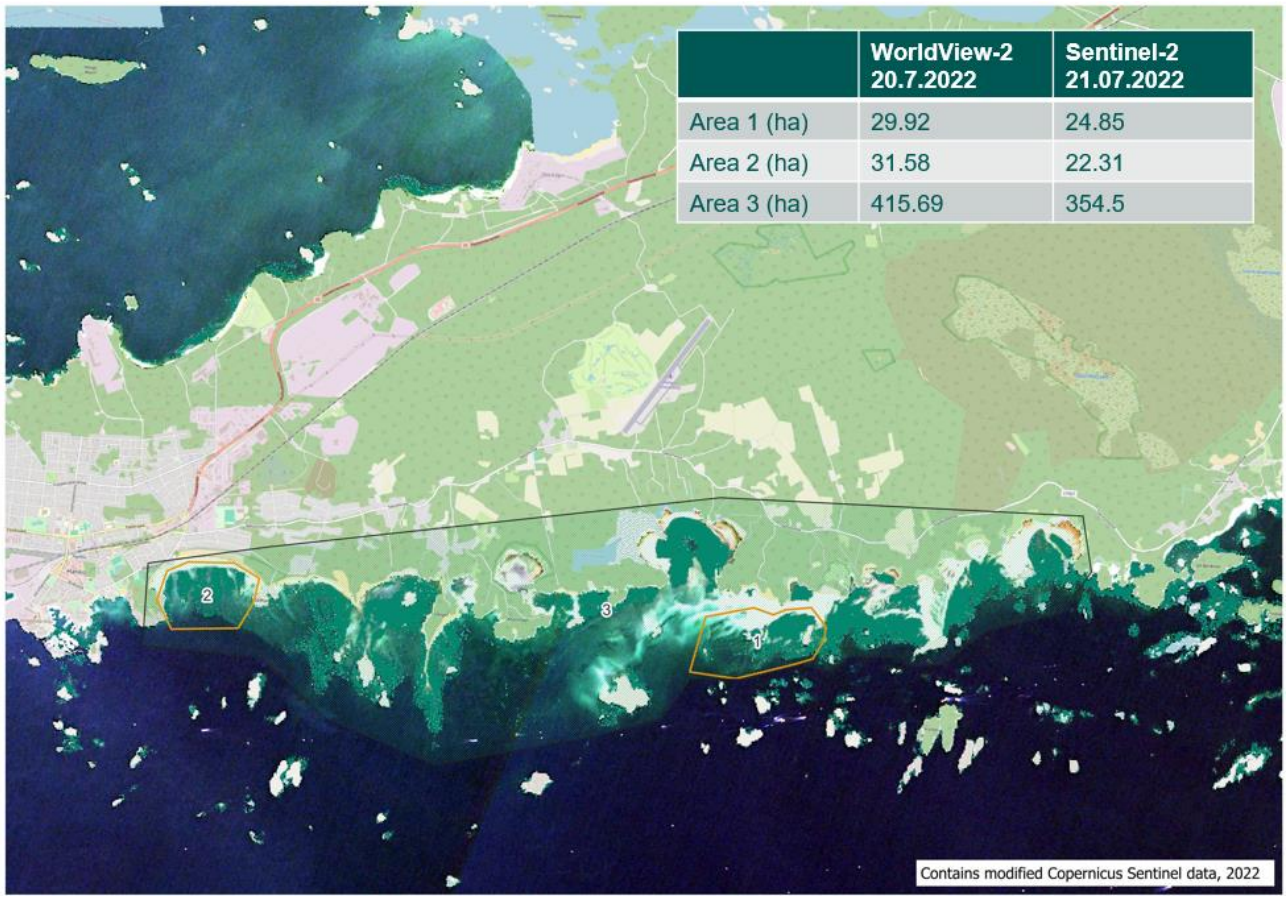

Figure 9. Comparison of areal extents from WV-2 and Sentinel-2 satellite data.

Summary

Mapping SAV extent on seagrass meadows performed well on both WV-2 and Sentinel-2 imagery. WV-2 showed higher accuracies which is likely due to the higher spatial resolution (2m) compared to Sentinel-2 (10m), as higher resolution sensors are capable to detect smaller scale fragmentation (Schütt et al, 2025). However, open access and continuous collection of Sentinel-2 data makes it very useful for large scale mapping of larger vegetation patches whereas the VHR satellite imagery may be used when more detailed mapping is needed.

Detecting the lower growth limit from echo sounding and dropvideo

The vegetation coverage of the site Kolaviken has been mapped within the Biodiversea project using remote sensing methods. The characteristic growth pattern of eelgrass (*Zostera marina*) on flat sandy and gravel substrates provides favorable conditions for the application of acoustic remote sensing techniques in monitoring these meadows. Due to water turbidity, optical remote sensing methods (e.g., drone RGB imaging) are often unsuitable during the growing season for mapping the lower boundary of the vegetation. To determine the lower limit of eelgrass beds, side-scan sonar and echo sounding were tested.

Echo Sounding Methods

The side-scan sonar system used was DeepVision DE3468D Dual 340/680 kHz (horizontal beamwidth: 0.9°/0.5°, vertical beamwidth: 60°/60°). The transducer was mounted securely to the vessel's side to ensure accurate sensor positioning. During side-scan sonar surveys, data was recorded using DeepVision DV5.0 software (license B10252), and positional information for the sonar was collected with a DIGITAL YACHT GPS160 USB TriNav GPS/GLONASS/Galileo receiver. Preliminary data processing was performed in

DeepVision DV5.0, while further analysis and interpretation of the lower vegetation boundary from sonograms were carried out in ArcGIS Pro, where the boundary was manually digitized. Side-scan sonar surveys for mapping the lower vegetation (Zostera marina) boundary were repeated in 06/2024, 09/2024, and 10/2025. In 10/2025, the position of the lower vegetation limit was determined using a high-precision echo sounder (DeepVision RTK Dual Frequency Down Scan, 700/200 kHz, 3° opening angle, AHRS).

Verification of Sonar Data

Acoustic data were verified through video recording (HD drop-video transects). For species verification, HD-video camera was used to confirm vegetation cover, species composition, and vegetation boundaries. As a more continuous alternative to point-based species observations, drop-video transects were tested as a new method to validate species presence and delineate the edge of continuous vegetation. Positioning was recorded with a Trimble TDC-6000 device (RTK) at 1–2 second intervals, with an average spatial accuracy of external RTK-antenna less than 5 cm.

Video recordings were captured in HD quality (GoPro Hero 5 Black, resolution 1080p, 30–48 fps, FOV Superwide, with flat lens dive housing). From the video footage, the following were analyzed: substrate type (Velmu classification), vegetation presence/absence, eelgrass coverage, other perennial vegetation species and coverage. A live video feed was transmitted to the surface via Wi-Fi, and the camera altitude was maintained at an appropriate level to ensure reliable identification of macrophyte species and eelgrass.

Results

Side-scan sonar data provide a reliable overview of eelgrass (Zostera marina) distribution down to the lower vegetation boundary, which is often beyond the reach of other remote sensing methods due to water turbidity. Simultaneous remote sensing data with field inventories from alternative sources may be limited because of factors such as satellite overpass schedules, cloud cover, water turbidity, wind, and wave conditions affecting drone imagery.

Interpretation of the lower eelgrass boundary from side-scan imagery was successful in 09/2024, even in cases where some drifting filamentous algae partially covered the vegetation. Based on these findings, surveys aimed at delineating the lower boundary should be conducted late in the growing season, when vegetation biomass is increased and boundaries within the mosaic community are more distinct. In early summer, abundant loose filamentous algae increase the likelihood of misinterpretation. In the case of Kolaviken, a single well-placed side-scan transect can provide spatially accurate data for the lower boundary (Figure 10).

Figure 10. Lower eelgrass boundary interpreted from side-scan sonar imagery. Aerial photographs © National Land Survey of Finland

Based on side-scan sonar results, all together 14 RTK down-scan transects were positioned along the lower boundary and verified lower growth limit using simultaneous HD-quality drop-video transects (Figure 11). On the sonar transects, the lower boundary of a continuous vegetation cover of the seagrass bed was on average at a depth of 5.7 meters (min 4,9 m and max 6,5 meters).

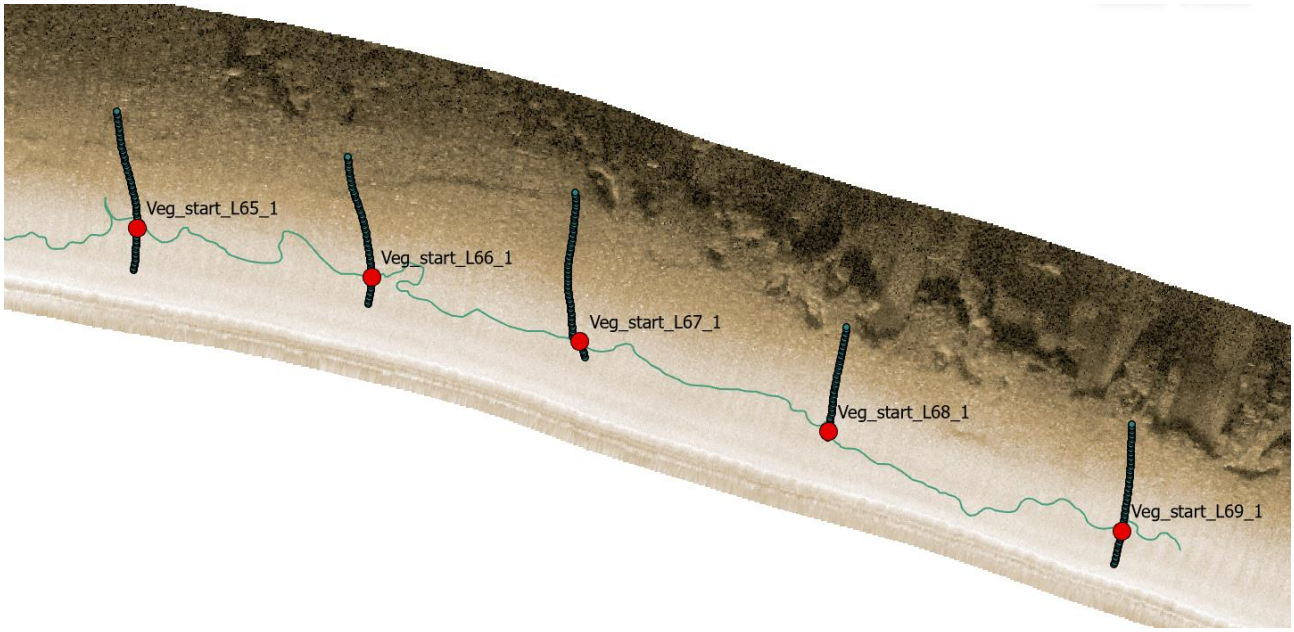

Figure 11. RTK down-scan transects were positioned along the lower boundary. Together with the HD-video transects confirmed lower boundary of the Kolaviken eelgrass meadow.

Comprehensive side-scan acoustic data can provide a good overall picture of changes in the distribution of the occurrence eelgrass meadows or detect structural changes eelgrass habitat in areas where optical remote sensing methods are not available, for example due to water turbidity. For more precise measurements and for ground truthing, a combination of high-resolution echo sounding and drop-video transects is recommended.

Changes within SAV coverage with aerial image time series

Study area

The study area is located in Kolaviken, Hanko, in the Southernmost peninsula of Finnish coast.

Aerial image dataset

The whole Finland is repeatedly covered with aerial images in every 3 to 5 years by NLS. This dataset offers feasible solutions to support operational monitoring of underwater habitats. The NLS dataset contains four repeated flights in Kolaviken (24042013, 14062017, 06062022, 14062025) with RGBN orthomosaics and a black and white ortho from 20042008. In addition MH holds aerial image datasets from Kolaviken from 30062002 and 14102014. In June 2024 the study area was flown with DJI Mavic 3M RTK drone at 120 meter altitude and spatially accurate orthomosaic was generated using OpenDroneMap software at CSC's Puhti supercomputer environment. Together, these datasets offer a nice opportunity to test how well aerial images can detect SAV and SAV dynamics in the study area.

NLS images are RGBN images with 50cm resolution. These images are offered freely in tiles and are within map like accuracy. MH images are RGB images with 30cm resolution and they are georeferenced manually to correspond the spatial accuracy of the NLS images. The drone orthomosaic is a RGB image with 5cm resolution.

We piloted the potential of mapping SAV dynamics in an area of interest (AOI) (Figure 12) within Kolaviken by calculating SAV area change from 2002 to 2024 and choosing a ten-year span from 2014 to 2024 to visually inspect the changes.

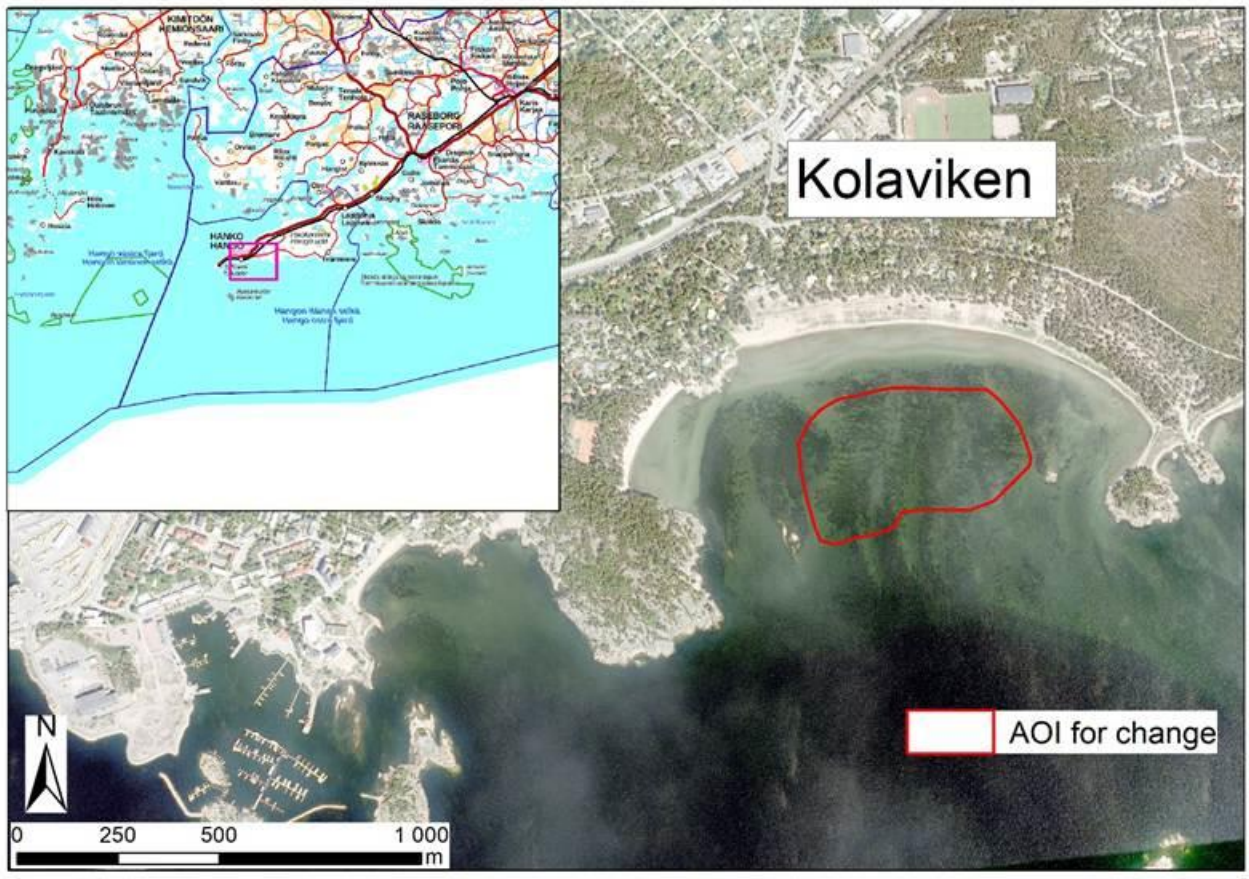

Figure 12. Study site and area of interest within Kolaviken. Base map and Aerial photographs © National Land Survey of Finland

Aerial image processing

The images were individually classified as SAV/no SAV. This was done first by segmenting the aerial images into segments. The segmenting considered spectral, spatial and minimum mapping unit (MMU) parameters. These parameters needed to be fixed on every image separately, as the conditions were not comparable. Our aim was to cover the SAV area with very small details to detect small changes in cover. Thus, we used very detailed segmenting approach.

Secondly, the segments were assigned as SAV or no SAV classes based on visual interpretation. These selected segments were used as training data for the SAV model. This is relatively straightforward interpretation based on the image. Next the segmented image was classified with Random Forest algorithm with default parameters. The accuracy of the SAV models was visually inspected by comparing them to corresponding aerial photograph and the segmentation procedure was repeated if any clear inaccuracies were found.

Change detection of SAV

The extent and spatial characteristics of SAV dynamics were calculated based on the built SAV models. To visualize the SAV dynamics along the time span of 2014 to 2024 the images coded and overlayed. Each layer is coded following multiplier 10^{n-1} (Table 2), where n is number of layers starting with the most recent.

Table 2. SAV model coding for overlay analysis

Image	SAV	no SAV
2014	10	0
2024	1	0

The spatial overlay enables detailed scrutiny of changes temporally and spatially. Code 11 in the overlaid dataset corresponds to permanent SAV and code 0 to permanent no SAV. The rest of the coding category refer to temporal changes in SAV i.e. increase, decrease.

Results

The SAV changes within the AOI in Kolaviken are shown in Table 3 below. The approach shows that the SAV area has been steadily increasing in Kolaviken.

Table 3. Total SAV extent within AOI from 2002 to 2024.

	2002	**2014**	**2017**	**2024**
SAV area	167678 m^2	232522 m^2	230418 m^2	254310 m^2

The spatial characteristics of SAV change are shown in the Figure 13 below. The change shows some clear spatial patterns while most of the SAV area has been permanent between 2014 and 2024.

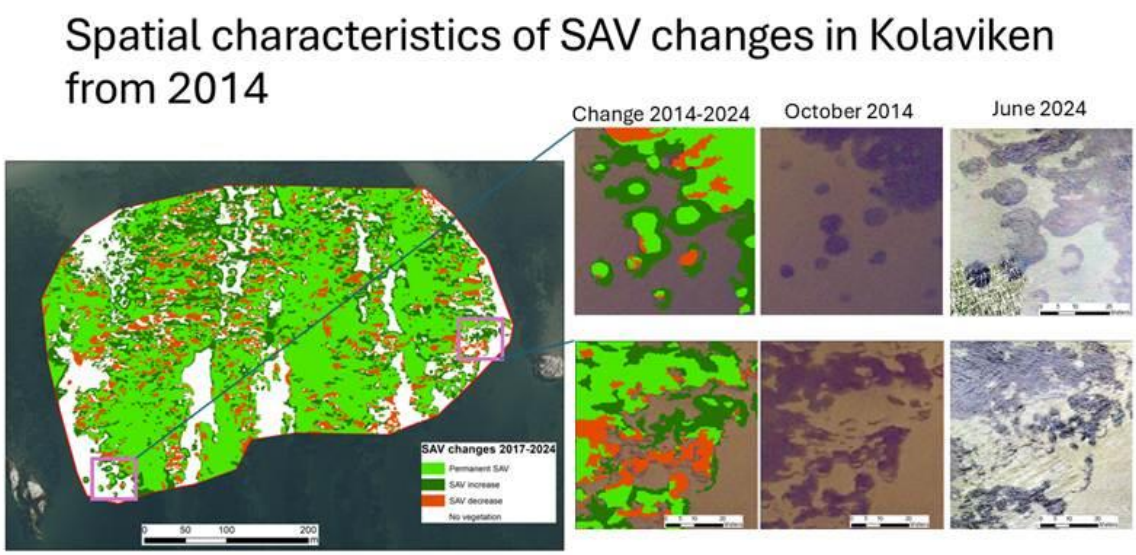

Figure 13. Spatial representation of SAV changes in Kolaviken AOI. Aerial photographs © National Land Survey of Finland

Conclusions

Aerial images are feasible and effective datasets to map the extent of SAV and its changes. Our piloted approaches were methodologically successful and offer robust methodology for SAV monitoring relying on NLS data. The NLS aerial image program offers operational monitoring standard within every 3 to 5 years and therefore creates a feasible backbone for monitoring SAV.

However, the aerial images cannot be used in interpreting SAV at species level. The next steps are to move from SAV to dominant species change. This can be done by sampling the vegetation and extrapolating the information based on SAV maps.

Furthermore, the timing of NLS aerial image is not suited for mapping underwater species. The images are often acquired in late spring/early summer, when SAV is not yet in full growth. Therefore, based on this pilot we suggest that the NLS aerial image catalogue should be complemented by acquiring additional aerial images from late summer.

Detailed echo sounding and drop video for estimating amount of Zostera marina within the meadow

Study area

The study area is located in Kolaviken, Hanko, in the Southernmost peninsula of Finnish coast.

Approach

The SAV models are informative in monitoring general vegetation extent and its dynamics. However, they are not providing information on the dynamics of species and their abundances which can indicate environmental changes. To move forward from SAV models to species level models, systematic and well-planned vegetation surveys are needed. Here, our aim is to develop approach for eelgrass cover estimation in Kolaviken.

The approach is based on dense sampling of a selected study areas within Kolaviken. The sample areas represent different sub-areas within the bay, referring to depth ranges and structure of SAV. During autumn 2025 two first test sites were selected and surveyed (Figure 14). The sample areas were surveyed using DeepVision RTK Dual Frequency Down Scan sonar that offer spatially accurate information on depth and vegetation height. In addition, underwater video footage was recorded with GoPro that is spatially linked to downscan sonar location data. This setting enables us to evaluate the extent and volume of SAV within the sample area, and also to estimate the cover of eelgrass and other species within the area. We will monitor the vegetation cover, height and species dynamics within the selected sample areas in the coming years.

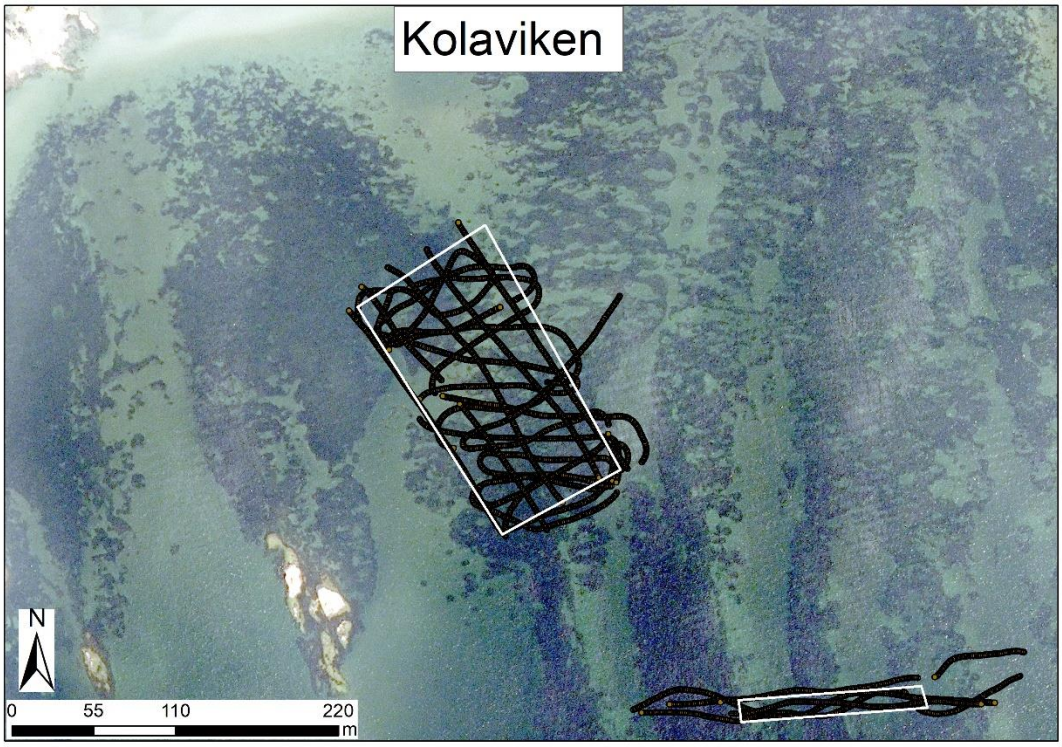

Figure 14. Sub areas and dense survey points in Kolaviken. Aerial photographs © National Land Survey of Finland

Habitat summary

SAV can be mapped using various optical remote sensing sensors in areas typical for seagrass meadows habitat where vegetation patches alternate with sandy substrate. Satellite missions such as Sentinel-2 have satellite overpasses every few days and therefore offer data that can be aligned temporally, but the 10-meter spatial resolution is unable to capture the small-scale changes. Colored aerial image or VHR satellite image archives can be used to acquire snapshots of past SAV extent with very high spatial resolution, yet challenges may arise from varying timing of aerial image collection in relation to vegetation growth peak, leaving some uncertainty to change detection and how much of the change is explained by seasonal variation. Studying the seasonal change that is observable from remote sensing sensors in seagrass meadows extent would help to remove uncertainty regarding comparisons over different years and seasons. Echo sounding may be used to detect lower growth limits where it is not identifiable from optical remote sensing. As differentiating eelgrass from other vascular plants within the meadow is not possible from optical remote sensing, drop video recording may be used to verify the habitat type. Piloting will continue to create monitoring time series and the combined use of different sensors.

Fucus habitats

Fucus beds can be found on hard rocky substrate across the Finnish coast from the eastern Gulf of Finland to Kvarken in the northern Bothnian Sea. This area has varying water conditions within sub-basins and notable differences in underwater geomorphology from steep cliffs to gentler slopes with varying substrate. These conditions make it difficult for one remote sensing method to be applicable for all areas and therefore different methods have been piloted in pilot sites (map).

Mapping Fucus beds from optical remote sensing imagery and point observations

Mapping Fucus from optical remote sensing images has been piloted on different spatial resolutions and sensors from drones to satellites. Based on existing research brown macroalgae has distinguishable spectral features (Kotta et al. 2014) and has been mapped with hyperspectral and multispectral sensors (Vahtmäe et al. 2021). However, water quality, depth and species composition affect how separable brown macroalgae is from other vegetation, green or red algae.

Study area

Using existing point observations to map Fucus has been piloted for a subregion near Pori in the Bothnian Sea (Figure 15). The area has extensive Fucus beds mixed in various degrees with other vegetation and seafloor varying between hard bottoms and soft sediment.

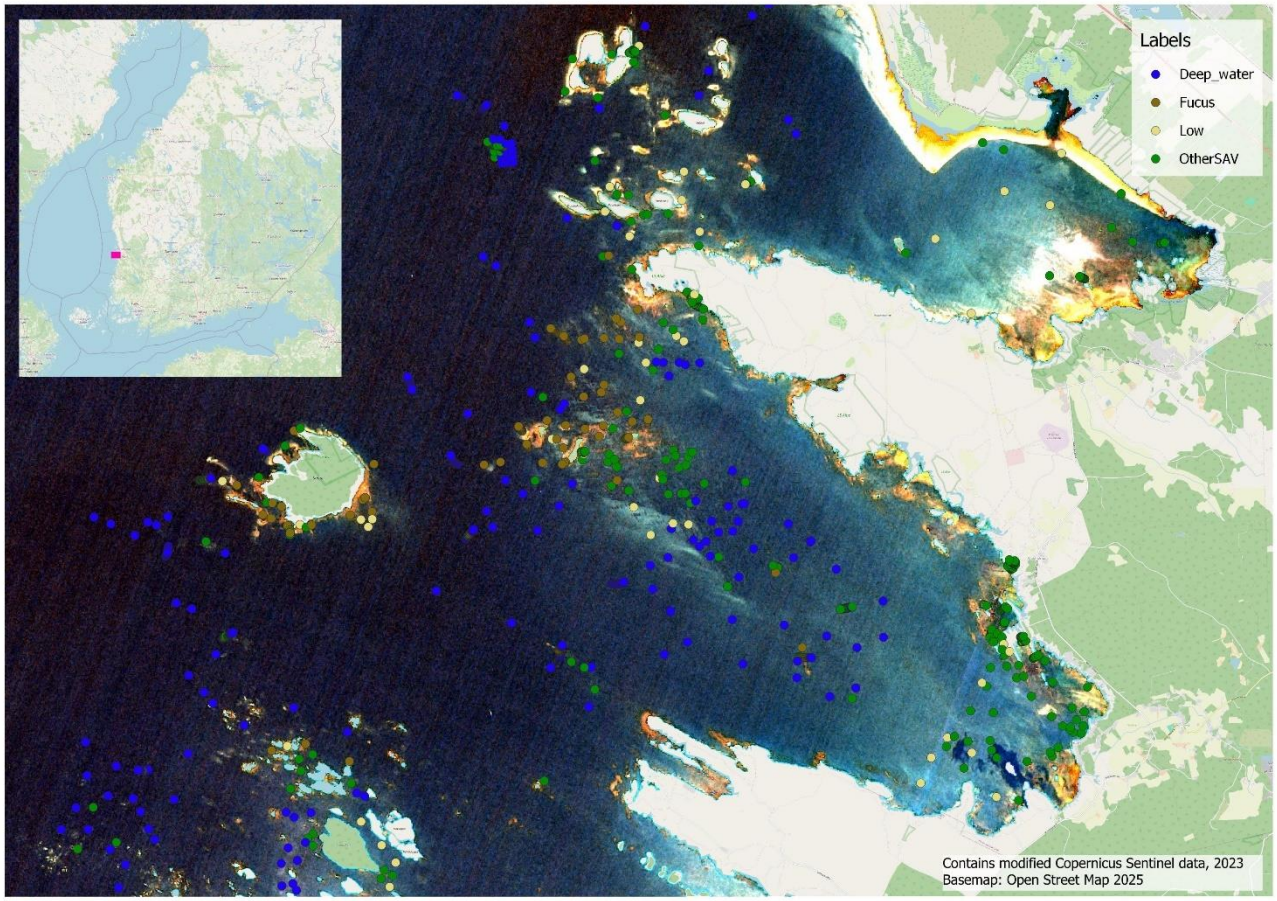

Figure 15. Map of study area with labelled Velmu point observations.

Data and methods

Velmu point observations from 2016-2023 were aggregated to broader semantic groups of brown algae, other SAV, bare or low vegetation cover seafloor, and deep water for image classification. Observations were

selected from a longer time span despite the temporal mismatch to satellite image to have enough observations of different classes at different depths over the pilot area. Also, Fucus is considered relatively stable perennial habitat except the most shallow areas susceptible to ice scouring, and therefore it was assumed that observations would be representative. Image classification was piloted on Sentinel-2 image from July 12th 2023, and for a Worldview-2 VHR satellite image from September 8th 2014. The points were used in similar OBIA workflow for satellite image classification as described in SAV mapping section. Spectral plot of Sentinel-2 pixels sampled to the points show how the spectral values averaged at 1-meter depth interval change between the classes at the pilot area (Figure 16).

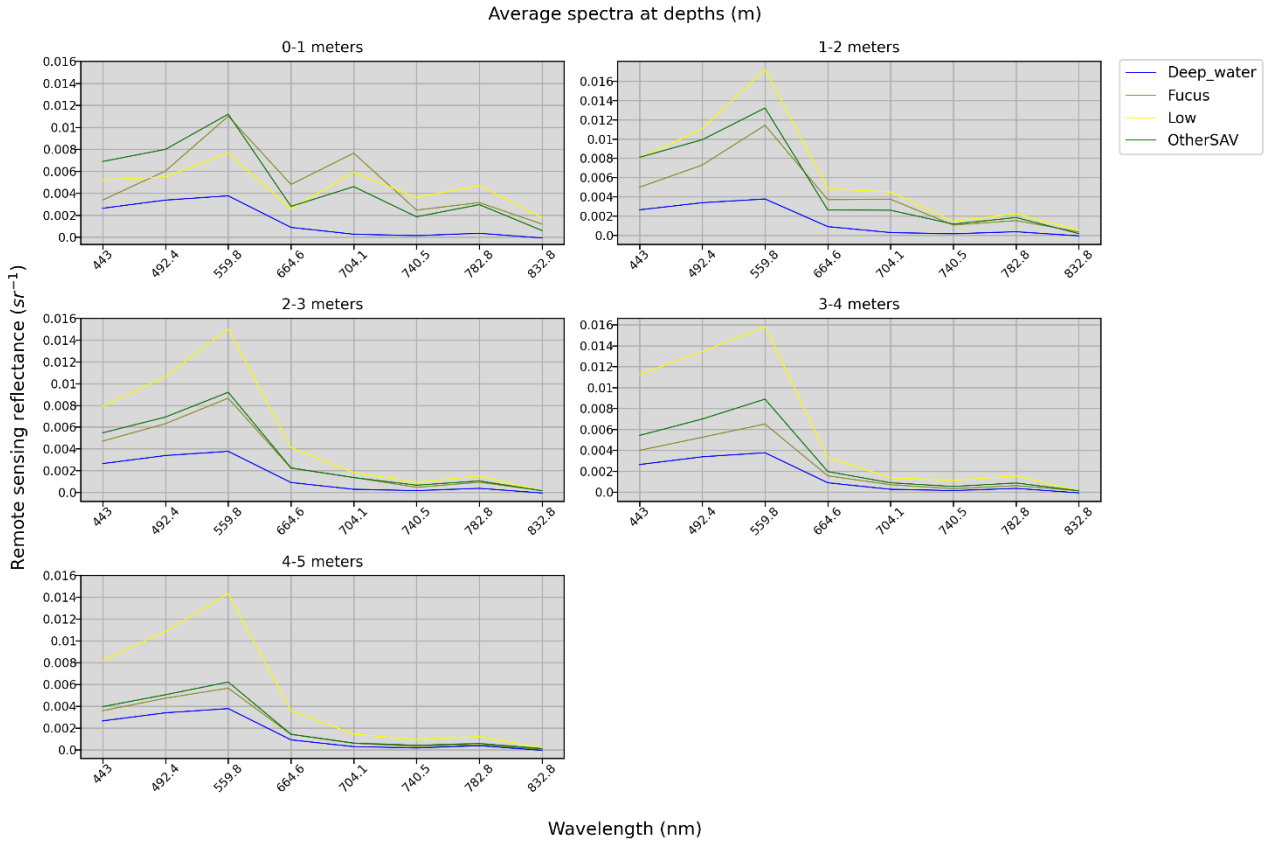

Figure 16. Spectral plot of Sentinel-2 pixels sampled at VELMU point observations in the study area and averaged to 1-meter depth intervals.Deep water class was added to each subplot as reference spectra for an area which is considered optically deep and light is not reflected from the sea floor.

Results and discussion

Extreme gradient boosting (XGB) model was used and its performance estimated in 10-fold grouped stratified cross-validation for both images (Table 4). Cross-validation results show that predictions made for unseen data have high uncertainty apart from deep water. This is likely due to spectral resemblance of classes.

Table 4. Cross-validated mean accuracy metrics for XGB image classification.

	Sentinel-2			VHR satellite (WorldView-2)		
	Overall accuracy 0,74	Precision	Recall	Overall accuracy 0,71	Precision	Recall
Deep		0,89	0,90		0,85	0,78
Fucus		0,45	0,27		0,68	0,61
Low		0,33	0,14		0,35	0,14
Other SAV		0,57	0,73		0,68	0,82

Higher spatial resolution seems to improve classification results especially for the vegetation classes. Low accuracy for low vegetation cover may be because of the class accounted for less than 10% of samples and that low vegetation cover may occur on different substrates that are not spectrally similar, e.g. mud, sand, or rock. After filtering misclassifications in deep water area, visual inspection of the Sentinel-2 prediction of Fucus probabilities show that predictions are located over vegetated patches and not randomly scattered (Figure 17).

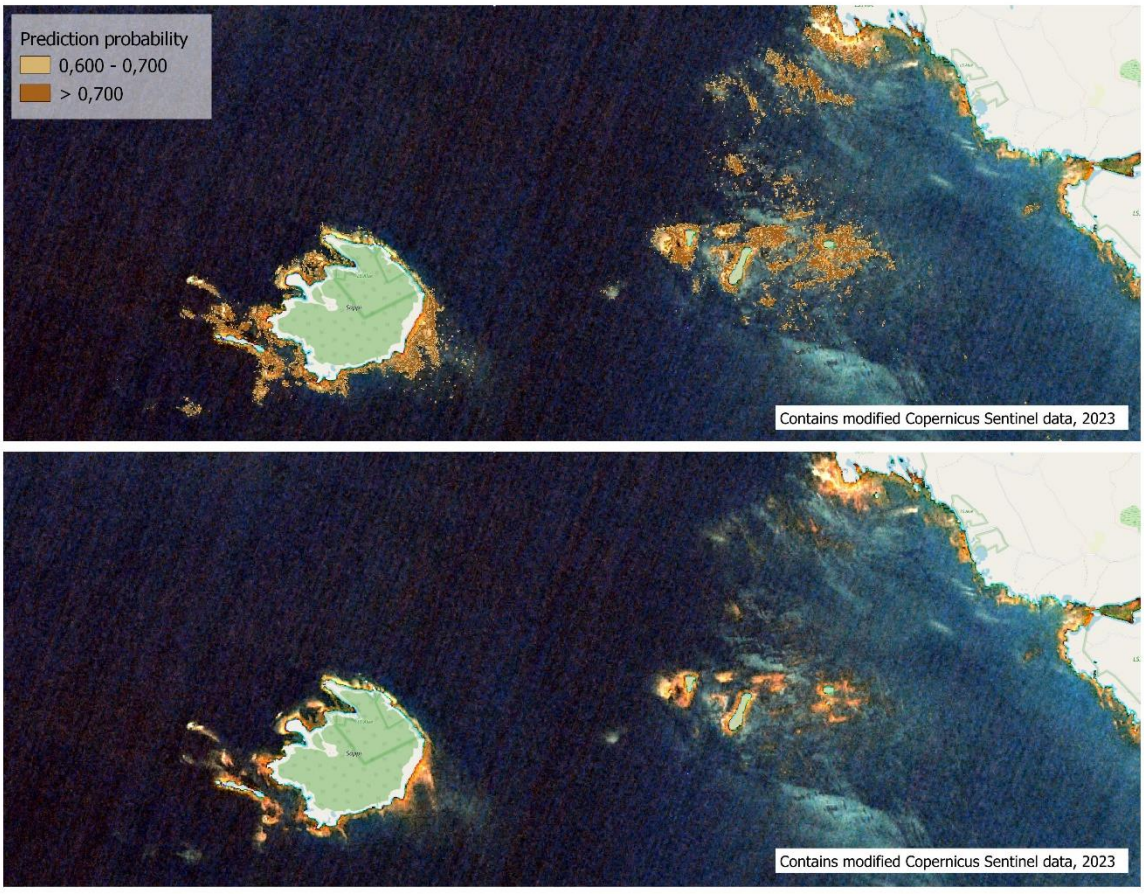

Figure 17. Predicted probability map for Fucus presence (above) and RGB visualization Sentinel-2 image (below) in pilot site.

A more detailed comparison of Fucus prediction probability maps to a drone orthomosaic shows that both satellite predictions align with areas that have Fucus cover, and predictions mostly avoid shallow water areas with low vegetation (Figure 18). However, as single drone orthomosaic can cover only relatively small area compared to satellites, similar validation should be done at different sites to have better estimate to what extent Fucus predictions are reliable.

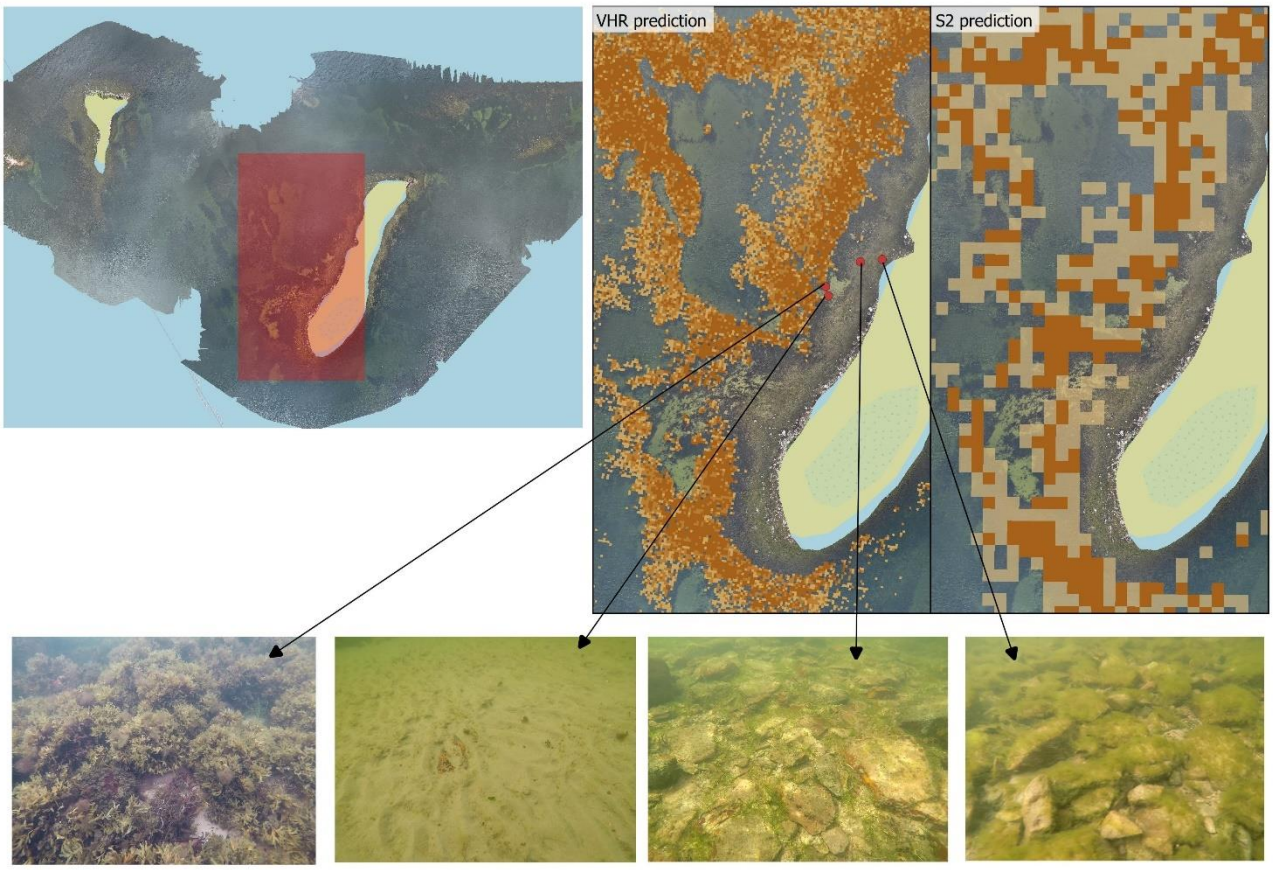

Figure 18. Fucus predictions from WorldView-2 and Sentinel-2 satellite images over drone orthomosaic. Underwater images show examples of different seafloor cover in the area. Underwater video was collected along with drone imagery and was done by wading from shore.

Using point-based field observations only to predict Fucus cover relies on samples collected from representative locations and at different depths to show the spectral differences between Fucus and other vegetation. Still, point observation may not account for variation in seafloor and vegetation cover at the pixel scale which leaves some uncertainty for training the model. Also, water conditions may vary between sheltered and exposed areas within single satellite image making predictions even more difficult. However, the examples show that despite uncertainties predictions can produce meaningful results. Further piloting is continued to develop methods and more extensive validation.

Upscaling drone information to larger spatial extent

Drone imagery was piloted to acquire very detailed information on wide Fucus belts and to use that in combination with coarser resolution satellite image to provide estimates of Fucus presence for larger area.

Data and methods

Drone imagery was collected between June 3rd and 7th in 2024 in northwestern Åland archipelago (Figure 19). Flights were done using DJI mavic 3M drone at 120-meter altitude and with minimum 75% frontal and side overlap. Five ground control points (GCP) were distributed across the mapping area and high accuracy RTK-GNSS coordinates were measured using Emlid Reach 2+ GNSS. Due to some connection issues during the flights the high accuracy RTK for the drone was disabled and the accurate image positions were post processed in RTKLib software using the observation and navigation information from FINPOS service by NLS.

Post processed image data was then imported with GCPs to Open Drone Map software which was used to compute the orthomosaics.

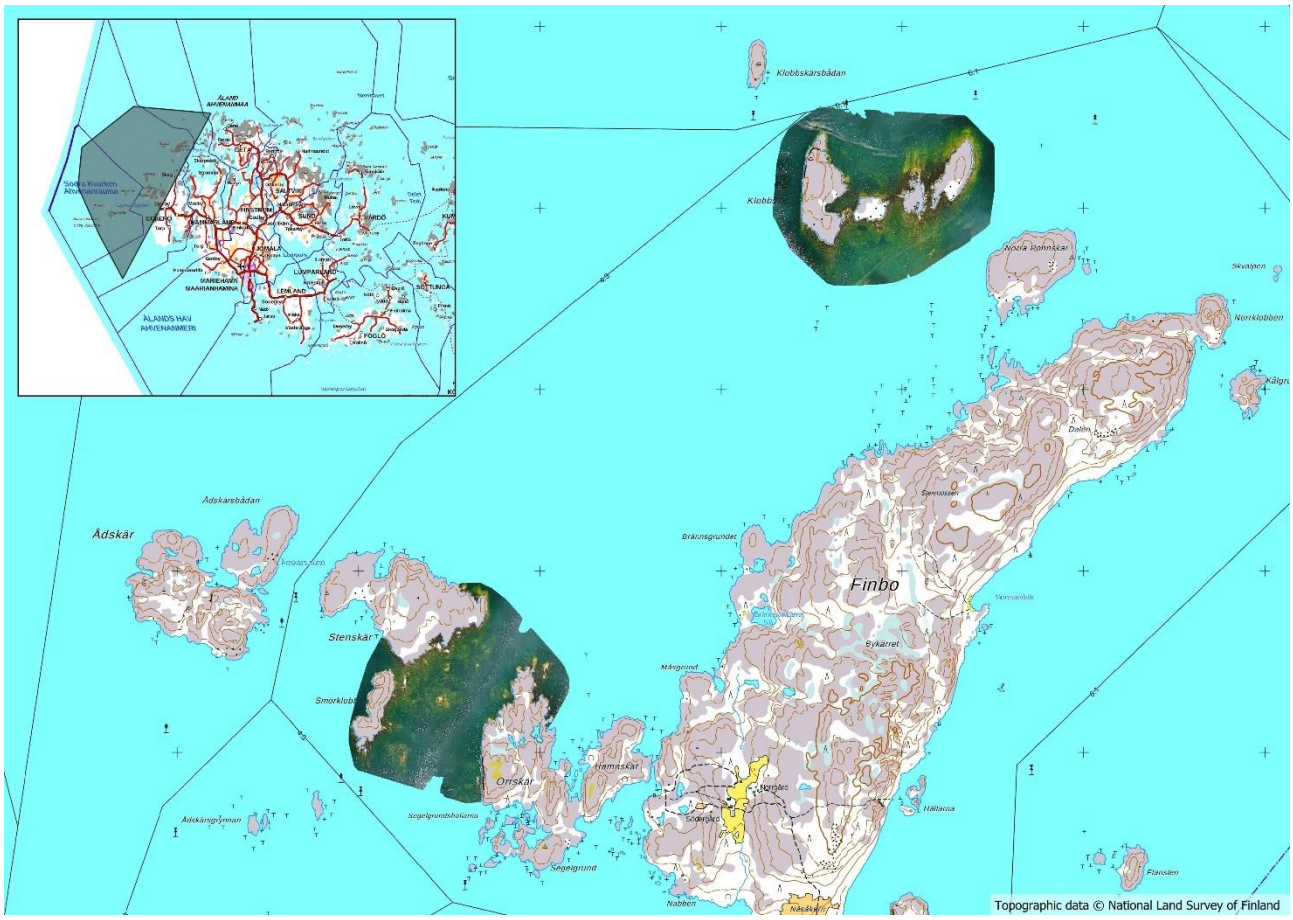

Figure 19. Map of the study area with two drone orthomosaics that were collected. The grey area in inset map shows the coverage of the Sentinel-2 tile that was used to test upscaling.

Dive and drop-video observations were used together with visual interpretation to annotate polygons of different habitat types for image classification. Image pixels were then extracted within the polygons and used in training machine learning models for image classification. Fucus prediction map from the drone orthomosaic was then aggregated to 10-meter grid polygons by computing mean coverage of Fucus in each grid cell. Grid cells with mean coverage >= 30% were used to train a model for predicting Fucus presence from Sentinel-2 image. Sentinel-2 tile T34VDM that covers the northwestern region of Åland was used from June 4th 2024, the same day the drone imagery was collected for training the model. Because of relatively small training dataset size from one drone mapping area, the results are at this stage compared visually to NLS aerial photographs and the second drone flight that was not used in creating training data.

Results and discussion

Fucus beds are quite separable in shallow water from bare rock but in deeper areas they are harder to distinguish from other vegetation or dark sea bottom features. Also, the Fucus beds in the drone orthomosaics seem to be most dense in the shallow water and become more scattered as the water depth increases. Image classification of drone orthomosaic performed with overall accuracy of 87%, and with precision of 85%, and recall of 97% for Fucus (Table 5).

Table 5. Confusion matrix and accuracy metrics for drone orthomosaic classification

	bare	deep	fucus	sav	Total	Precision
bare	30190	0	2975	1284	34449	0,92
deep	0	3557	1007	24	4588	0,96
fucus	266	161	29324	455	30206	0,85
sav	2312	4	1368	2458	6142	0,58
Total	32768	3722	34674	4221	75385	
Recall	0,88	0,78	0,97	0,40		
Overall accuracy	0,87					

Aggregating the drone prediction map to Sentinel-2 spatial resolution and selecting the pixels with mean cover => 30% resulted in 12720 pixels to train a model for classifying the Sentinel-2 image (Figure 20). A random forest model with default settings was used for classification.

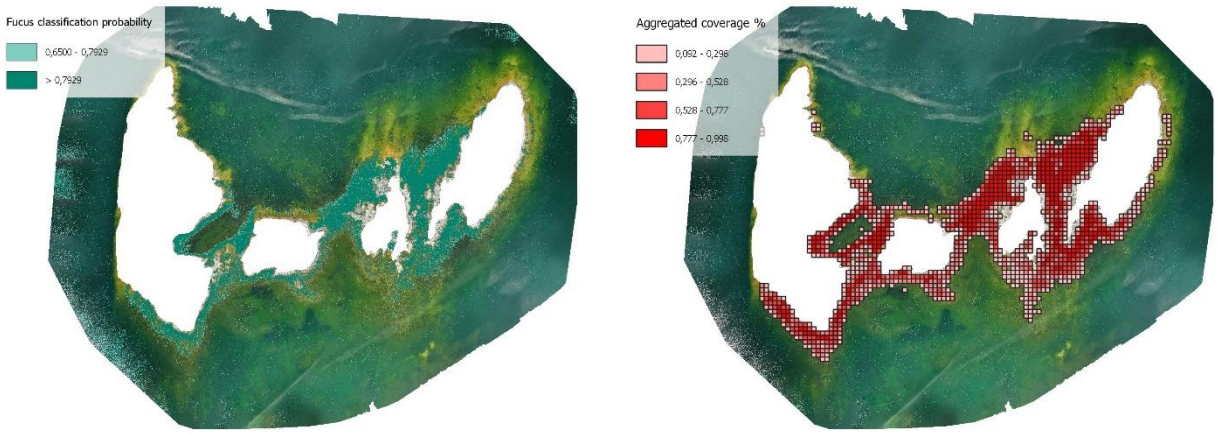

Figure 20. Drone orthomosaic with classified Fucus probabilities (left) and aggregated coverage percentage to Sentinel-2 resolution (right).

Visual comparison of Sentinel-2 prediction map and higher resolution aerial images show that predictions mostly occur in regions that can visually be interpreted as likely Fucus beds (Figure 21). However, predictions do not capture the same areal extent that is interpretable from the high-resolution images, thus leading to underestimation of areal extent. This may be caused by the relatively small training dataset where samples are located in quite shallow water. Nevertheless, the demonstrated workflow shows promise in extracting very high spatial resolution information from drone imagery and upscaling that to coarser satellite resolution.

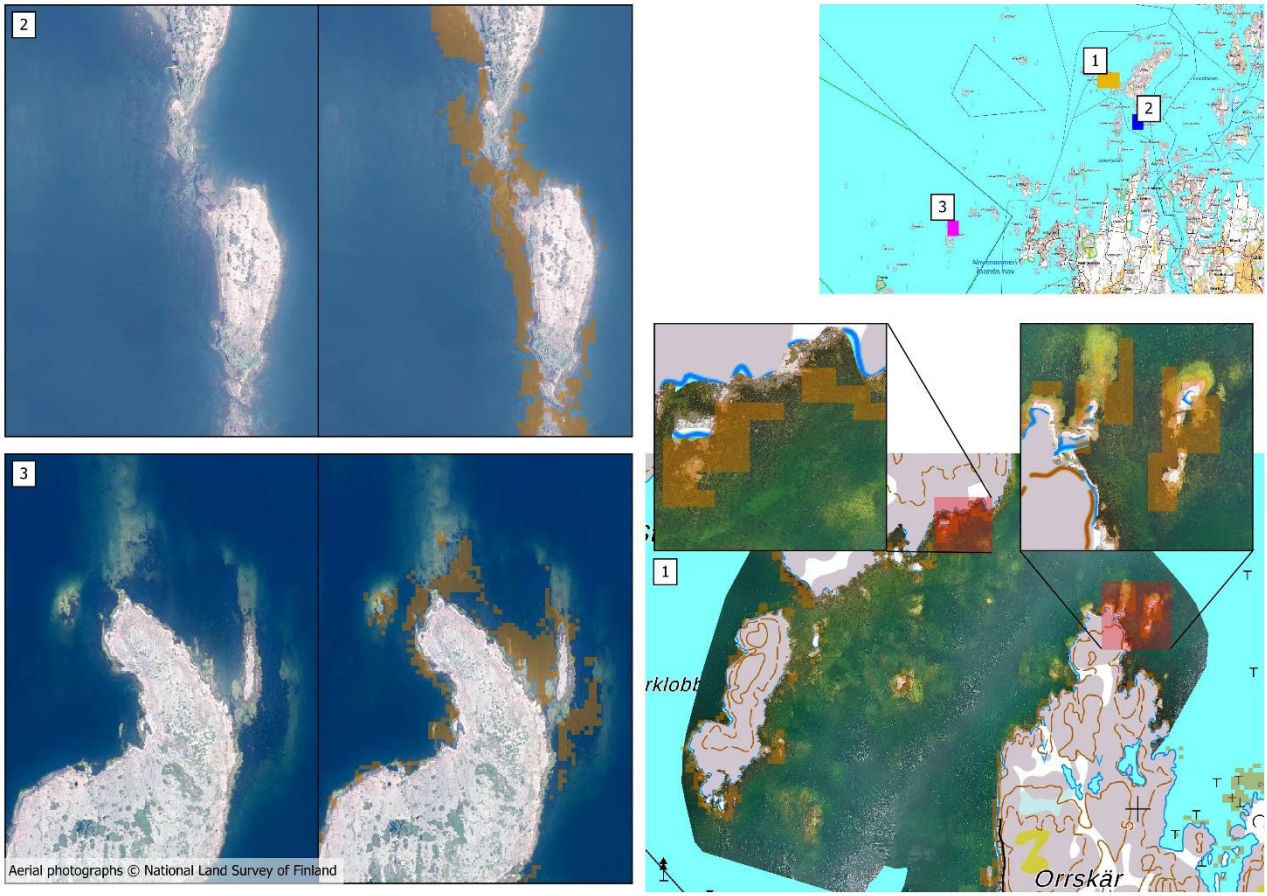

Figure 21. Sentinel-2 prediction of Fucus presence using the drone derived training data. The colored rectangles in the top right map show the locations of the sample plots.

Next steps for developing the described method would be to expand the drone classification of Fucus to as deep areas as possible, use more training data for Sentinel-2 classification by combining information from both drone mapping areas and test different models, make more thorough validation of the Sentinel-2 prediction. The method could also be piloted in other sea areas, for example Bothnian Sea, and with other optical remote sensing data.

Summary of optical remote sensing of Fucus

Mapping the extent of Fucus using optical remote sensing is challenging as the spectral signal is easily mixed to other vegetation especially when water depth increases. In addition, a single 10 by 10-meter pixel may consist of a mosaic of various habitats instead of continuous Fucus monoculture, creating a mixed signal which may lead to inaccuracy and uncertainty when combining point observations to pixel information. However, pilot studies show that satellite sensors may provide meaningful predictions. Drones provide very high-resolution data that can be used to create training samples that correspond to spatial resolution of other remote sensing sensors which could be used to map Fucus in shallow waters over large spatial extents. Piloting is continued to improve models and validation, and to develop combined use of drones and other remote sensing imagery.

Detection of Fucus beds using acoustic methods

Echo Sounding Methods

The side-scan sonar system used was DeepVision DE3468D Dual 340/680 kHz (horizontal beamwidth: 0.9°/0.5°, vertical beamwidth: 60°/60°). The transducer was mounted securely to the vessel's side to ensure

accurate sensor positioning. During side-scan sonar surveys, data were recorded using DeepVision DV5.0 software (license B10252), and positional information for the sonar was collected with a DIGITAL YACHT GPS160 USB TriNav GPS/GLONASS/Galileo receiver. Preliminary data processing was performed in DeepVision DV5.0, while further analysis and interpretation of the suitable bottom substrate was carried out in ArcGIS Pro, where the boundary was manually digitized.

In 11/2025, the position of the lower vegetation limit for bladderwrack was determined using a high-precision echo sounder (DeepVision RTK Dual Frequency Down Scan, 700/200 kHz, 3° opening angle, AHRS) together with simultaneous HD-video transects.

Verification of Sonar Data

Side-scan sonar datasets were validated using 42 vegetation transects. In addition, during the 2025 season, further analyses will compare high-resolution down scan sonar data with the 2024 diving transect dataset (42 transects) as well as with other high-resolution video transect outputs. Species verification was carried out using so-called video transects, which confirmed the presence of bladderwrack (*Fucus vesiculosus*) along the simultaneous down scan sonar data.

As a more continuous and spatially comprehensive alternative to point-based species verification, a new method—drop-video transects—was tested. These were used to confirm species composition and delineate the boundaries of continuous vegetation stands. The video recordings were of HD quality (GoPro Hero 5 Black, resolution 1080p, 48 fps, FOV Superwide, flat lens in a dive housing). Live footage from the drop-video was transmitted to the surface via Wi-Fi, and the camera altitude was maintained at an appropriate level to ensure reliable identification of macrophyte species.

Results

The resolution of the side-scan sonar was not sufficient to delineate bladderwrack stands; instead, the data were used to interpret bottom substrate suitable for bladderwrack within the target area. The total area surveyed with side-scan sonar was approximately 34 hectares, of which about 15 hectares were digitized as suitable substrate for bladderwrack (Figure 22). During interpretation, no depth model with adequate resolution for the area was available. Therefore, the lower depth limit of bladderwrack stands will be determined in subsequent analyses using appropriate models and vegetation transects (42 transects).

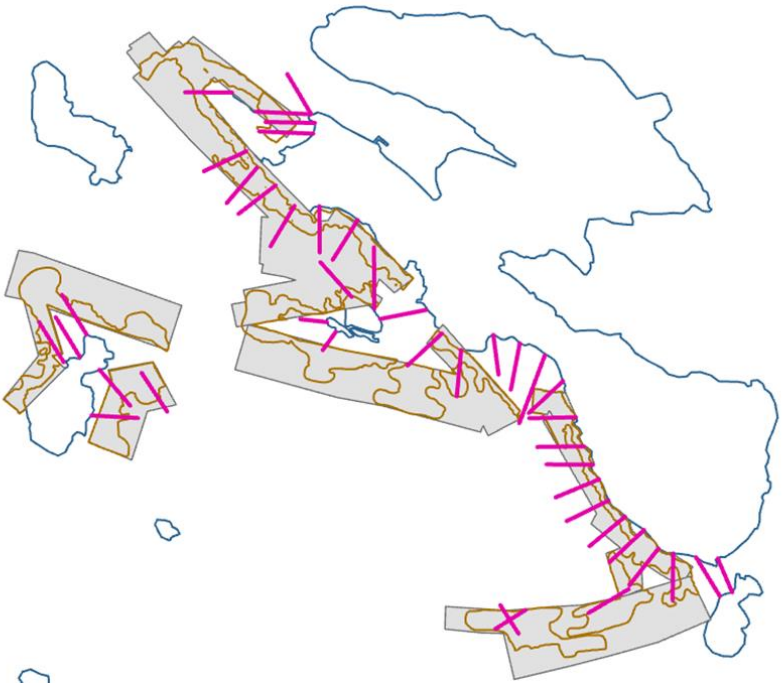

Figure 22. Areas surveyed with side-scan sonar (grey). Planned locations of vegetation transects (pink lines; 42 transects, each 100 m long), and bottom substrate suitable for bladderwrack (Fucus vesiculosus), interpreted from side-scan sonar imagery (brown delination)

Additionally, during the 2025 season, side-scan sonar data interpretation was validated using high-resolution down sonar and HD video transects. A total of 33 high-resolution sonar transects were surveyed, of which 29 were verified at their shallow sections using HD video transects.

Detailed analyses are still ongoing, but preliminary results indicate that high-resolution sonar is best suited for measuring the height of bladderwrack stands on flat substrates (i.e., smooth bedrock). In contrast, on bottoms typical of the Ulko-Tammio area—characterized by large boulders and stones—depth variations produce uneven bottom profiles in the sonar data.

Stoneworts

Sheltered stonewort habitats

Study area

The study area is located in Ruskiavuorenaukko, Uusikaupunki SW Finland (Figure 23). Ruskiavuorenaukko is a typical shallow water lagoon system in SW Finland experiencing high human pressure from the vicinity due to leisure boat traffic. Based on previous observation of NLS aerial image catalogue, submerged aquatic vegetation is abundant and somewhat permanent in the area. Since the lagoon system is ideal environment for charophyte communities, Ruskiavuoreanukko is a very potential place for charophyte existence and thus hosts an interesting location for testing charophyte mapping via drones.

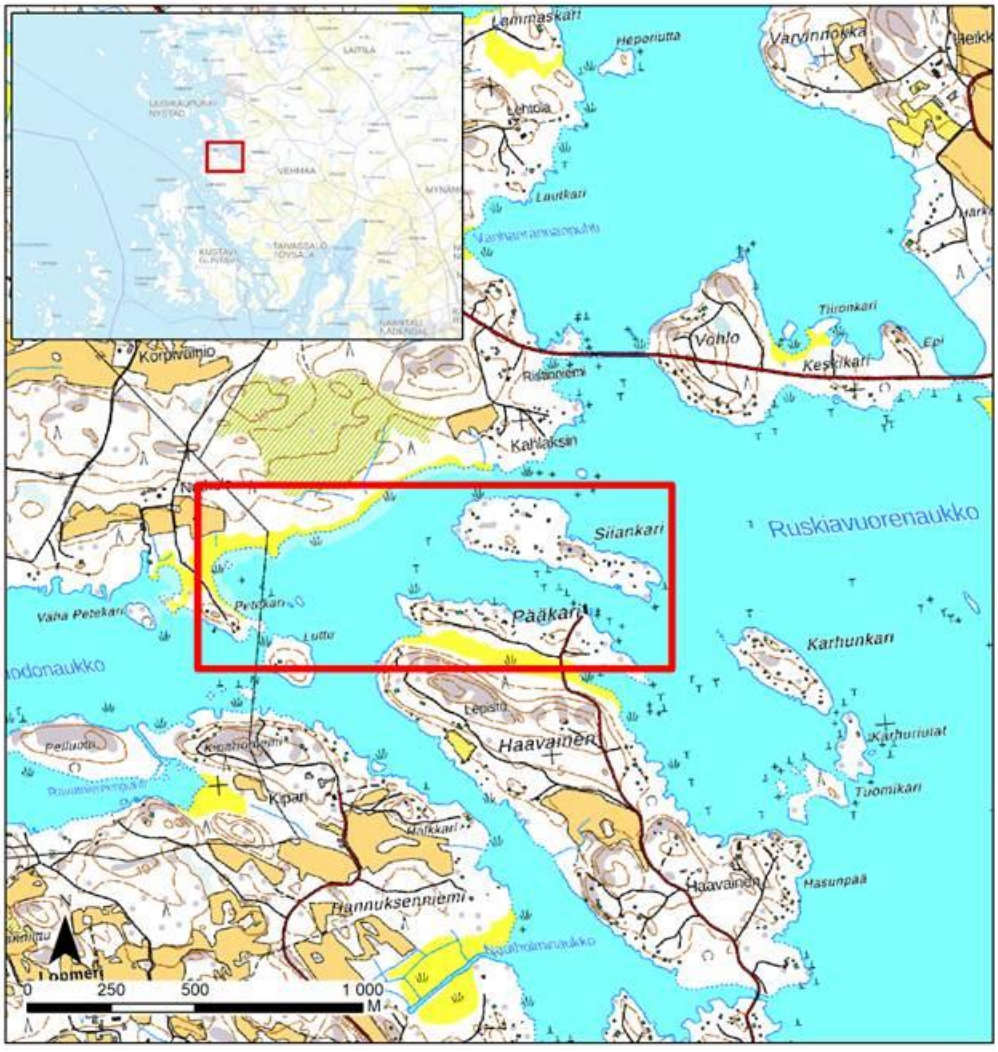

Figure 23. The study area. Topographic data © National Land Survey of Finland

Drone imaging

We used DJI Mavic 3 Multispectral drone for image acquisition in the study area. The Mavic 3 M is mounted with 20MP RGP sensor and 5MP multispectral bands (Blue, Green, Red, InfraRed, RedEdge). We used only the RGB sensor for the image acquisition.

The Flight was executed on July 2nd early in the morning to minimize the effects of sun glint and refraction. The flight path was planned according to the sun direction, following the protocol for mapping shallow water habitats suggested by Joyce et al. (2018). However, we allowed the drone to capture images also when the flight direction was facing the sun. We used 50m as flight altitude to avoid spatially too detailed mapping as we were interested to test the potential of drone imaging to recognize habitat dominant species. With 50m altitude the pixel size is still very detailed, ca inch per pixel. we used 75% as side and frontal overlap to optimize the following photogrammetric modelling.

Drone image processing

The drone images were further processed into orthomosaic in ESRI Site Scan application. Site Scan offers only a few options for decision prior processing and the actual photogrammetric procedure is a "black box" with no possibilities for adjustments. The georeferenced orthomosaic was further processed in ArcGIS Pro software. The orthomosaic was segmented based on spectral and spatial attributes. Segmentation merges pixels together according to the parameters set by the user. With drone imagery, segmentation prior further modelling reduces the computing time compared to original pixel-based approach. The segmentation parameters were chosen based on visual interpretation referring to the original orthomosaic.

Reference data collection

Reference data was collected on July 2nd with semi-autonomous surface vehicle mounted with Lowrance Elite 9 chartplotter, downscan sonar sensor and depth adjustable GoPro 11 camera. The vehicle offers options to preplanned route development for mapping or manual mapping. The plotter is equipped with GPS receiver and records location in every half a second. The vehicle enables rapid mapping of relatively large and shallow areas providing location-based information on depth, vegetation height and structure and video footage of the habitat.

In total 2 hours of video and ca 2000 sample plots with depth were collected for reference and validation purposes.

Modelling and validation

Training schema was designed based on the overall representation of the orthomosaic. Training segments were assigned to classes based on visual interpretation referring to original image. The classes were assigned as: Charales dense, Charales sparse, Bare bottom, Very shallow/Rock, Shadow and Turbid. The shadow class was created as drone image contained some tree shadows that are not spectrally corresponding to underwater habitat.

The assigned segments were used to model the segmented image. Random forest classifier with default settings were used as modelling approach.

Individual validation dataset was created based on the collected reference data. Ten points overlapping each class were chosen randomly and the model accuracy was assessed.

Results

The stonewort dominated community is clearly seen from the drone image and the classified model is representing well the habitat extent by visual judgement (Figure 24).

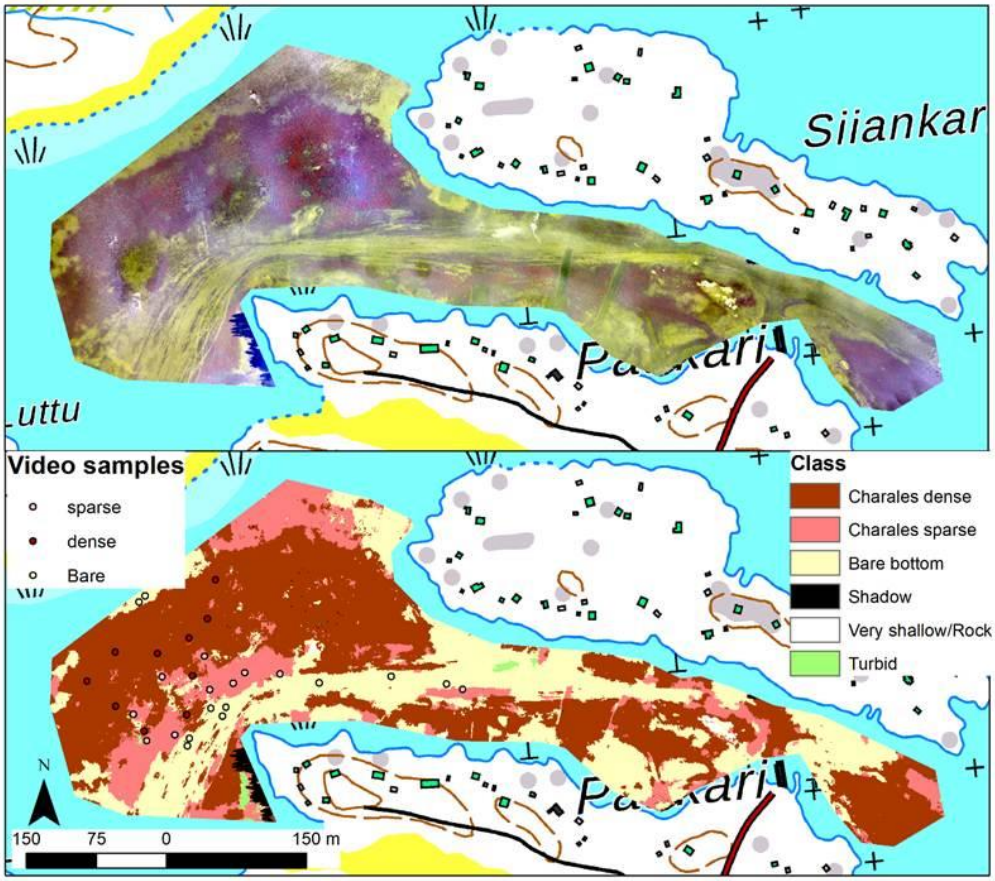

Figure 24. Drone classification. Topograhic data © National Land Survey of Finland

The video sample frames are shown below.

Figure 25. Sample images from the class Charales dense

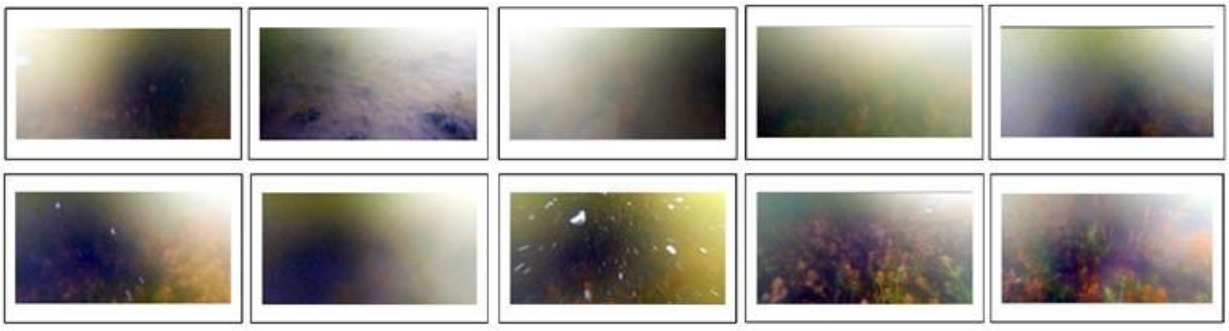

Figure 26. Sample images from the class Charales sparse

Figure 27. Sample images from the class Bare bottom

Based on the samples the overall accuracy of the model is 77%. The lowest accuracy is within Charales sparse class, which is a challenging class to determine with the used methodology. The underwater camera is facing front, and it is not always clear to interpret the vegetation cover, especially as the water is turbid at times. If the classes are merged and the model is tested only for vegetation/no vegetation the overall accuracy is 83%.

Exposed stonewort habitats

Stoneworts in the Bothnian Bay may form continuous vegetation covers also in exposed areas where these may be identifiable from remote sensing imagery as SAV. However, the dark water colour in the Bothnian Bay limits the optical remote sensing method to very shallow areas, and preliminary field work indicates that stonewort habitat may cover vast areas that are not visible in optical remote sensing imagery. Therefore, a combination of remote sensing mapping and echo sounding with drop-video will be piloted for mapping the exposed stonewort habitats in Bothnian Bay.

Conclusions

Here we show that satellite and drone based remote sensing approaches, combined with underwater acoustic and imaging methods are promising for monitoring the extent of submerged marine habitats, as well as coastal reeds. The main results from piloted methods are summarized in Table 6. These approaches will offer efficient tools to support the monitoring needs of the EUs Nature Restoration Regulation. These methods will also support the development of Essential Biodiversity Variables, especially those focusing on ecosystem extents.

Table 6. Summary of results for piloted habitats

Habitat	Objective	Piloting result
Reed beds	Extent monitoring	Satellite based Bayesian data analysis method has been developed that can be used to monitor reed bed coverage outside shoreline
Seagrass meadow		
Optical remote sensing	Extent	Multiple examples show that SAV can be mapped from remote sensing imagery which allows the monitoring of seagrass meadow extent. Differentiating the proportion of seagrass from other plants within the meadow is not feasible.
Echo sounding with drop-video	Lower growth limit, height, condition	Acoustic methods can be used to delineate lower growth limit of seagrass meadows and to measure vegetation height. Possibilities for condition assessments with video data.
Fucus beds		
Optical remote sensing	Extent	Piloted methods indicate potential to map wide Fucus belts, but methods need more development and validation to be applicable for large areas.
Echo sounding with drop-video	Lower growth limit, height, condition	Fucus stands are not easy to identify from echo sounding data, but suitable substrate can be identified. Fucus height is measurable on smooth bedrock surfaces but more challenging amongst boulders and rocks of varying size.
Sheltered stonewort habitats (lagoon)	Extent	Mapping has been demonstrated with drone imagery. *Chara tomentosa* is possible to separate by spectral signal
Exposed stonewort habitats	Extent, (condition)	Initial tests indicate that SAV mapping from remote sensing combined with acoustic field mapping can be used to estimate stonewort extent. Possibilities for condition assessment from drop-video to be piloted.

Acknowledgements

We wish to thank following partners for collaboration during the piloting work.

FINMARI – Finnish Marine Research Infrastructure.

University of Helsinki Tvärminne Zoological Station for collaboration in CoastalBiomon project led by Camilla Gustafsson.

Åbo Akademi for collaboration in use of Husö biological station and equipment during field data collection

The authors wish to acknowledge CSC – IT Center for Science, Finland, for computational resources.

References

Forsblom, L., M. Azhar, L. J. Barkved, D. Berov, T. Børsen, A. Cenci, S. De Innocentiis, V. G. Fonseca, et al. 2024. Review of existing and emerging techniques for benthic habitats. *OBAMA-NEXT project deliverable*. Zenodo. doi:10.5281/zenodo.14099051.

Forsblom, L., Virtanen, E. A., Arponen, H., Boman, R., Haapamäki, J., Hoikkala, J., Kallio, N., Karvinen, V.-J., Kaskela, A., & Keskinen, E. (2024). Finnish inventory data of underwater marine biodiversity. *Scientific Data*, *11*(1), 1297.

Jonne Kotta, Kalle Remm, Ele Vahtmäe, Tiit Kutser, & Helen Orav-Kotta. (2014). In-air spectral signatures of the Baltic Sea macrophytes and their statistical separability. *Journal of Applied Remote Sensing*, *8*(1), Art. 1. https://doi.org/10.1117/1.JRS.8.083634

Joyce, K. E., Duce, S., Leahy, S. M., Leon, J., & Maier, S. W. (2018). Principles and practice of acquiring drone-based image data in marine environments. *Marine and Freshwater Research*, *70*(7), Art. 7.

Koponen, S., Väkevä, S., Jokinen, A.-P., Virtanen, E., Viitasalo, M., Blenckner, T., and Cervo, A. de: Blue Carbon Habitats - a comprehensive mapping of Nordic salt marshes for estimating Blue Carbon storage potential, https://doi.org/10.6027/temanord2022-506, 2022.

Schütt, E. M., Uhl, F., Schubert, P. R., Reusch, T. B. H., & Oppelt, N. (2025). Mapping subtidal seagrass in the turbid Baltic Sea: Rethinking satellite sensor selection using a sensor-agnostic pipeline. *Science of Remote Sensing*, *11*, 100243. https://doi.org/10.1016/j.srs.2025.100243

Vahtmäe, E., Kotta, J., Lõugas, L., & Kutser, T. (2021). Mapping spatial distribution, percent cover and biomass of benthic vegetation in optically complex coastal waters using hyperspectral CASI and multispectral Sentinel-2 sensors. *International Journal of Applied Earth Observation and Geoinformation*, *102*, 102444. https://doi.org/10.1016/j.jag.2021.102444